minerals

MDPI

Article

Two Distinct Fractional Crystallization Mechanisms of A-Type Granites in the Nanling Range, South China: A Case Study of the Jiuyishan Complex Massif and Xianghualing Intrusive Stocks

Wenzhou Xiao [1,2], Chaoyun Liu [3], Kaixuan Tan [1], Xianzhe Duan [1,*], Kaituo Shi [1], Qinglin Sui [1], Peng Feng [1], Mabrouk Sami [4], Mohamed S. Ahmed [5] and Feng Zi [6,*]

1 Hunan Key Laboratory of Rare Metal Minerals Exploitation and Geological Disposal of Wastes, School of Resource Environment and Safety Engineering, University of South China, Hengyang 421001, China; lilzhou@usc.edu.cn (W.X.); nhtkx@126.com (K.T.); 2022000063@usc.edu.cn (K.S.); fengpeng@usc.edu.cn (P.F.)
2 Fundamental Science on Radioactive Geology and Exploration Technology Laboratory, East China University of Technology, Nanchang 330013, China
3 Key Laboratory of Metallogenic Prediction of Nonferrous Metals and Geological Environment Monitoring, Ministry of Education, School of Geosciences and Info-Physics, Central South University, Changsha 410083, China; liuchaoyun0718@126.com
4 Geology Department, Faculty of Science, Minia University, El-Minia 61519, Egypt; mabrouk.hassan@mu.edu.eg
5 Geology and Geophysics Department, College of Science, King Saud University, P.O. Box 2455, Riyadh 11451, Saudi Arabia; mohahmed@ksu.edu.sa
6 School of Earth Sciences and Spatial Information Engineering, Hunan University of Science and Technology, Xiangtan 411201, China
* Correspondence: duanxianzhe@126.com (X.D.); zifeng@hnust.edu.cn (F.Z.)

Abstract: The petrogenesis of A-type granites with different occurrences in the Nanling Range remains unclear. In this study, a case study of the Jiuyishan complex massif and Xianghualing intrusive stocks was conducted to determine this problem. The Jiuyishan complex massif is composed of four units (Jinjiling, Pangxiemu, Shaziling and Xishan). These four units have similar zircon U-Pb ages of approximately 153 Ma, with high Zr + Nb + Ce + Y contents (>350 ppm), high 10,000 Ga/Al ratios (>2.6), and a high crystallization temperature, indicating A-type affinities. They show a gradual change in lithology and geochemistry, implying a fractional crystallization process. These units also have similar εNd(t) values (−8.2 to −5.8) and zircon εHf(t) values (−7.5 to −2.2) except for the Shaziling MMEs (mafic microgranular enclaves) (−14.2 to 4.8), demonstrating their lower crustal source. However, the Shaziling unit may have contributed mantle-derived magma based on the geochemical data of its hosted MMEs. In comparison, the two Xianghualing intrusive stocks have similar geochemical features but exhibit highly evolved features (high Rb, U, Y, Ta and Nb contents and low Eu, Ba, Sr, P, Ti, Ca, Mg and Fe contents, with V-shaped REE distribution patterns). They have different zircon U-Pb ages of approximately 160 Ma and 155 Ma. The two stocks also have similar whole-rock εNd(t) values (−6.5 to −5.7) and zircon εHf(t) values (−7.6 to −2.7) and equally illustrate a lower crustal source region. Combining with their vertical zonation, they may have experienced remarkable fractional crystallization with possible assimilation processes. We propose that the Jiuyishan complex and Xianghualing stocks have two distinct fractional crystallization mechanisms during their formation. The Jiuyishan complex was formed by in situ crystal mush fractionation, while the Xianghualing stocks were formed by flowage differentiation during magma ascent or gravitational settling during magma solidification after emplacement. However, more than one mechanism affected the fractional crystallization processes of these granitic rocks.

Keywords: Jiuyishan; Xianghualing; A-type granite; complex massif; intrusive stocks; fractional crystallization mechanisms

check for updates

Citation: Xiao, W.; Liu, C.; Tan, K.; Duan, X.; Shi, K.; Sui, Q.; Feng, P.; Sami, M.; Ahmed, M.S.; Zi, F. Two Distinct Fractional Crystallization Mechanisms of A-Type Granites in the Nanling Range, South China: A Case Study of the Jiuyishan Complex Massif and Xianghualing Intrusive Stocks. *Minerals* **2023**, *13*, 605. https://doi.org/10.3390/min13050605

Academic Editor: Jaroslav Dostal

Received: 23 March 2023
Revised: 19 April 2023
Accepted: 25 April 2023
Published: 27 April 2023

1. Introduction

The concept of A-type granite was first proposed by Loiselle and Wones [1], with the three basic features being "Alkali, Anhydrous, and Anorogenic". The granites that conform to the initial definition of A-type granites typically have extremely high temperatures, high alkali and low water content [2–6]. However, the "A-type" concept has already been broadened, and granites with only high alkali features are also called A-type. In this case, a large number of highly evolved granites, with high alkali contents but low crystallization temperatures and a high water content, were also regarded as A-type granites [7–11]. Under the circumstances, the relationships between the traditional A-type granites and highly evolved A-type granites have still not been precisely and exhaustively researched.

A large number of A-type granites in the Nanling Range can be divided into two occurrences [12,13]. The most developed occurrence is a complex massif, while the majority of complex massifs are composed of several large-scale A-type granitic batholiths (>100 km^2). Within the complex massif, each single pluton can be spatially and temporally related or lithologically and geochemically linked [14–16]. The other occurrence is intrusive stock. In such situations, A-type intrusive stocks are spatially isolated and usually highly evolved, and vertical lithology zonation can be identified from the hidden bottom to the exposed top of these stocks [17–21]. Despite several occurrences of A-type granitic rocks in the Nanling Range, the different formation mechanisms between the complex massif and intrusive stock are still poorly understood, especially the formation of correlated units in complex massif and lithology zonation in intrusive stocks. The lack of such research, particularly on their source, protolith and fractional crystallization mechanism, leaves an obstacle to understanding the petrogenesis and metallogenic processes of A-type granites.

In the Nanling Range, multiple A-type granites with ages of 160–150 Ma have been discovered with different occurrences [12,13,22]. Located in the western Nanling Range, the Jiuyishan complex massif (composed of four units) and the Xianghualing intrusive stocks (two isolated stocks) are two representative A-type granitic rocks with different occurrences, and they are excellent objects to study their different formation mechanisms. In this paper, a comparative study of petrology and geochemistry of these two occurrences was carried out, including zircon U-Pb dating, whole-rock geochemistry and Sr-Nd-Hf isotopes. We attempted to determine the petrogenesis of these two occurrences and the relationship between different lithologies in different units. The case study can provide better information for understanding the petrogenesis and metallogenic processes of A-type granites.

2. Geological Background and Sample Description

2.1. Regional Geology

The South China block is combined with two Precambrian blocks, namely, the Yangtze block in the northwest and the Cathaysia block in the southeast (Figure 1a). These blocks amalgamated during the Neoproterozoic along the arc-shaped Jiangnan orogenic belt [23–25]. The South China block collided with the North China Craton in the north in the Triassic, and continental collision formed the high-pressure metamorphic orogenic belt called the Qingling-Dabie orogenic belt [26,27]. The Songpan-Ganzi block consists of several micro blocks that were gradually amalgamated onto the South China block during the Triassic after the Qingling-Dabie orogenic belt was formed [28,29].

The Nanling Range is located in the southwestern part of the Cathaysia block. The exposed strata of the Nanling Range are almost completely from the Ediacaran to the Quaternary, but the Silurian is absent (Figure 1b). The Ediacaran strata mainly consist of sandstone and metasandstone and are only sporadically distributed. The Cambrian strata consist of sandstone, metasandstone and slate and are distributed mainly around the Jiuyishan district. The Ordovician strata consist of slate at the bottom and limestone on the top, and they are covered by the Devonian and Carboniferous carbonate rocks, which are the most widely developed strata in this area. The Permian and Triassic strata mainly consist of limestone, dolostone and shale. Only sporadic Jurassic to Quaternary strata is exposed [30].

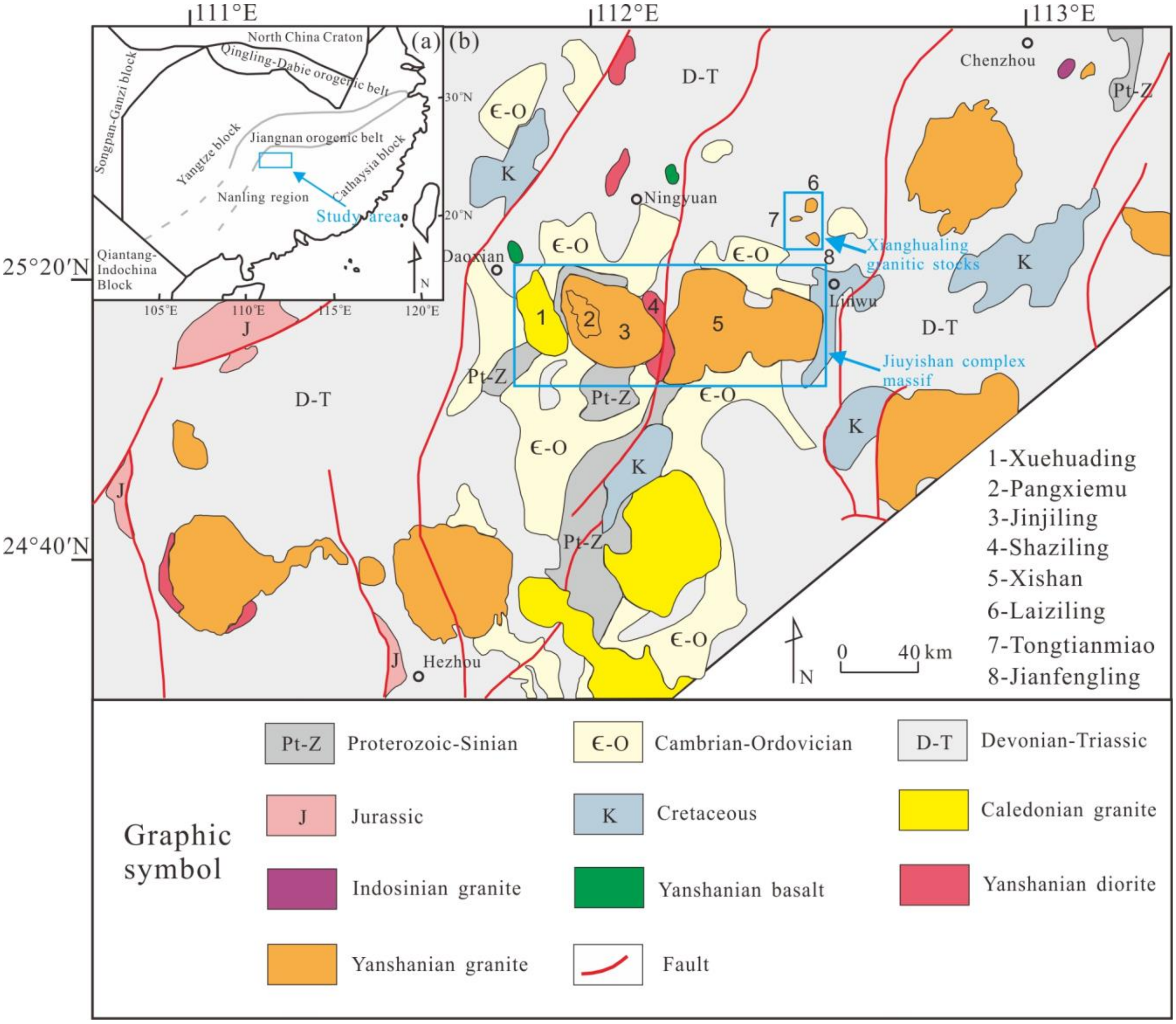

Figure 1. (**a**) Geological map of the South China block (Modified after Liu et al. [10]); (**b**) Geological map of the Nanling Range (Modified after Shu et al. [12]).

Fractures and folds are strongly developed in the Nanling Range (Figure 1b), with several regional deep fractures that control the distribution of magmatic rocks. The deep fractures are mainly NE-trending in the northern area but become NW-trending in the southern area. However, folds are usually EW-trending and accompanied by magmatic intrusions [12]. Granitic rocks, diorite and mafic rocks are widely distributed in this region (Figure 1b). Early Paleozoic granites are commonly S- and I-type granites; they are less abundant and formed large intrusions, corresponding to the Caledonian intracontinental orogenic event in South China [31]. Early Mesozoic granites are also S- and I-type granites; they are the least common and formed small intrusions, triggered by the amalgamation of the North China Craton and the South China Block in the Triassic period [21]. Late-Mesozoic granites are most commonly developed in this area, which are usually A-type granites and accompanied with cotemporaneous basalts and diorites, corresponding to the intraplate extension triggered by the roll-back of subducted paleo-pacific plates in the Jurassic period [31].

2.2. The Jiuyishan Complex Massif

The Jiuyishan complex massif is located in the southwestern Nanling Range and composed of five units (Figure 1b). Each unit is distributed from west to east with different shapes and lithologies. The westernmost unit, called Xuehuading (Figure 2), is composed of granodiorite, monzonitic granite, and biotite granite, with zircon U-Pb ages of between 432–412 Ma [31–33], and was formed much earlier than the other four units. Abundant, dark enclaves were discovered in the Xuehuading unit. These MMEs are dark gray, with sizes ranging from 5–10 cm. The MMEs commonly occur as lobate shapes and do not show evidence of any reaction with the host magma, and were likely formed by mafic mineral aggregation during magma ascent rather than mantle magma injection [31]. The Xuehuading granite has protoliths of Paleoproterozoic metaigneous and metapelitic rocks, with an I-type affinity [33].

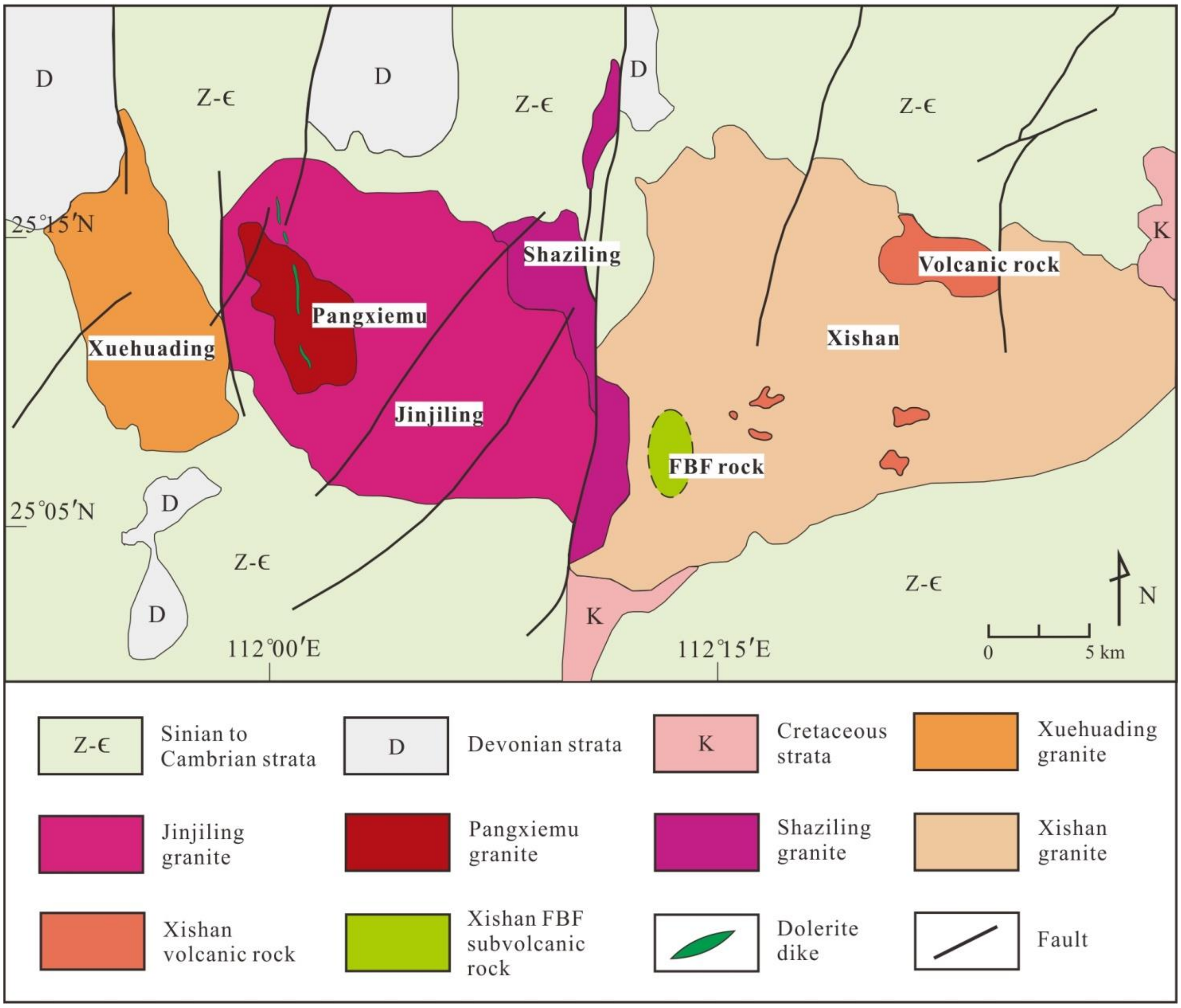

Figure 2. Geological map of the Jiuyishan area (Modified after Guo et al. [3]).

The Jinjiling unit is located to the east of the Xuehuading unit; no contact zone was observed between them. The Pangxiemu unit intrudes inside the Jinjiling unit (Figure 2); no quenching band can be observed, but pegmatite, quartz veins and greisens are developed around the contact zone [34]. The Jinjiling unit has zircon U-Pb ages of between 159–153 Ma and is composed of biotite granite with porphyritic textures [10,32,34]. The Jinjiling unit has protoliths of lower-crustal granulitic metasedimentary rocks, exhibiting an A-type affinity [10]. The Pangxiemu unit has zircon U-Pb ages of between 153–146 Ma and is composed of zinnwaldite granite [10,34]. The Pangxiemu unit has the same source region as the Jinjiling granite and exhibits an A-type affinity with a much higher fractionation degree [10].

The Shaziling unit is located between the Jinjiling and the Xishan volcanic-intrusive complex with a strip shape (Figure 2), which is composed of granodiorite and monzogranite with a porphyritic texture, with zircon U-Pb ages of between 157–153 Ma [32,35]. Abundant, mafic enclaves also appear and show features of MMEs. These MMEs are commonly ovoid, ellipsoidal and angular in shape, with sizes of several centimeters–meters. The MMEs have sharp contacts with their host granite, but no obvious chilled borders have been observed. The Shazling MME sample has a zircon U-Pb age of 152.1 $\pm$ 1.1 Ma and variable εHf(t) values (-14.2 to 4.8), indicating mantle magma injection [35]. The Shaziling granite has protoliths of lower crustal graywacke or pelite and exhibits an A-type affinity [35].

The Xishan volcanic-intrusive complex is located in the easternmost part of the Jiuyishan complex massif (Figure 2) and is composed of three units: granitic rocks, volcanic rocks and fayalite-bearing felsic (FBF) subvolcanic rocks. The granitic rocks occupied the largest area of the Xishan complex; the volcanic rocks are exposed in two main areas inside of the granitic rocks, with one exposed in the northwestern margin with a very large area and another exposed in the middle of the granitic rocks with several sporadic minor areas. The FBF subvolcanic rocks were developed in the southwestern part of the granitic rocks with an oval-shaped area (Figure 2). The Xishan granite has zircon U-Pb ages of between 156–154 Ma [2,32] and is composed of biotite granite and granite porphyry, having protoliths of Paleoproterozoic metasedimentary and metaigneous rocks with an A-type affinity [2,36]. The Xishan volcanic rocks are mainly dacites, rhyolites, tuffs and fragmentary lavas, and have geochemical and isotopic features similar to the Xishan granites, indicating an A-type affinity [32]. The Xishan FBF rocks were formed via the mixing of two batches of magma, which have two groups of zircons U-Pb ages: 152 Ma and 157 Ma. The FBF rocks were formed under extreme conditions of high temperature, low–moderate water contents, and low oxygen fugacity [3].

A dolerite dike developed inside the Jinjiling and Pangxiemu units with a zircon U-Pb age of 153 Ma. It was formed by the partial melting of the garnet-bearing lithospheric mantle, which experienced metasomatism of the underplating asthenospheric mantle melts [37].

2.3. The Xianghualing Intrusive Stocks

Located in the northeast area of the Jiuyishan complex massif, the Xianghualing area is composed of four small granitic intrusions (<5 km^2) and four felsic dikes (Figure 3). The Jianfengling and Laiziling stocks are the two largest intrusions in this area, and they are generally referred to as the Xianghualing intrusive stocks. The Laiziling stock is located on the north side of the area with an oval shape, while four nearly EW-trending felsic dikes are distributed on its east side and west side. The Jianfengling stock is located on the south side of this area with a nearly triangular shape; in its northwest part, a tiny stock called Yaoshanli is present. The Tongtianmiao stock is on the top of the dome with a nearly oval shape (Figure 3). Due to the local geographical conditions (high altitude without accessible roads), Tongtianmiao and Yaoshanli are located in positions that are difficult to visit, so few reports about them have been published.

The Laiziling and Jianfengling granites are highly evolved A-type granites with source regions in the lower crust, and they have zircon U-Pb ages of between 156–150 Ma [9,12,19,38–40] and 165–160 Ma [9,41], respectively. Both the Laiziling and Jianfengling granites show vertical zonation and contain different lithologies from bottom to top: biotite granite at the bottom, zinnwaldite granite in the middle, and topaz–albite granite and greisen at the top [17,19,20,38,42–45].

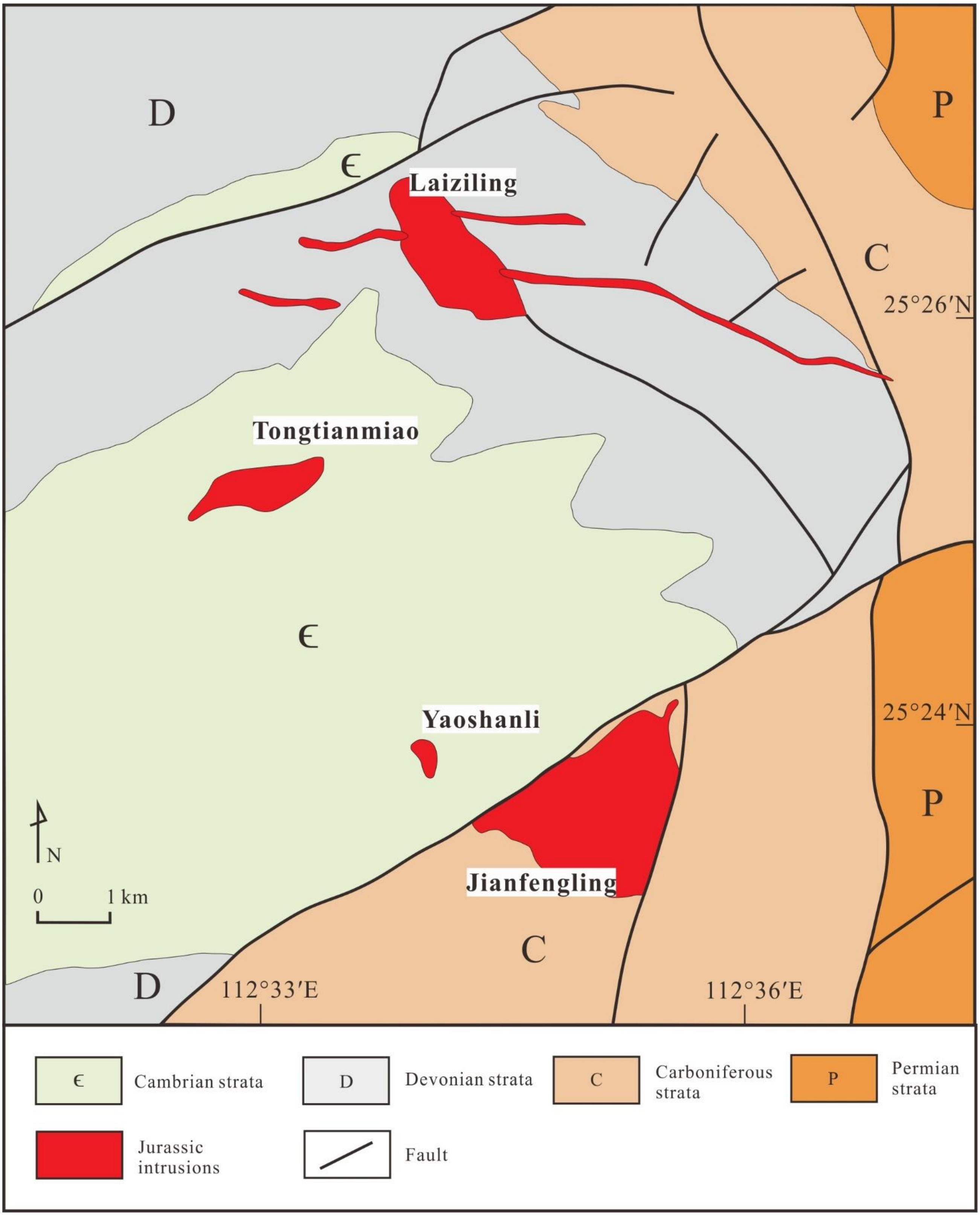

Figure 3. Geological map of the Xianghualing area (Modified after Qiu et al. [46]).

2.4. Sample Description

The Jinjiling unit is mainly composed of medium-to-coarse-grained biotite granite. The samples of the Jinjiling biotite granite are massive and light-gray-to-whitish colored, with porphyritic textures (Figure 4a). The groundmass has particle sizes of approximately 2–10 mm, consisting of quartz (35%–40%), plagioclase (20%–25%), K-feldspar (25%–30%) and biotite (~5%), with accessory minerals of zircon, titanite and ilmenite (Figure 4b). The phenocrysts are mainly composed of plagioclase and K-feldspar, with particle sizes of approximately 5–25 mm.

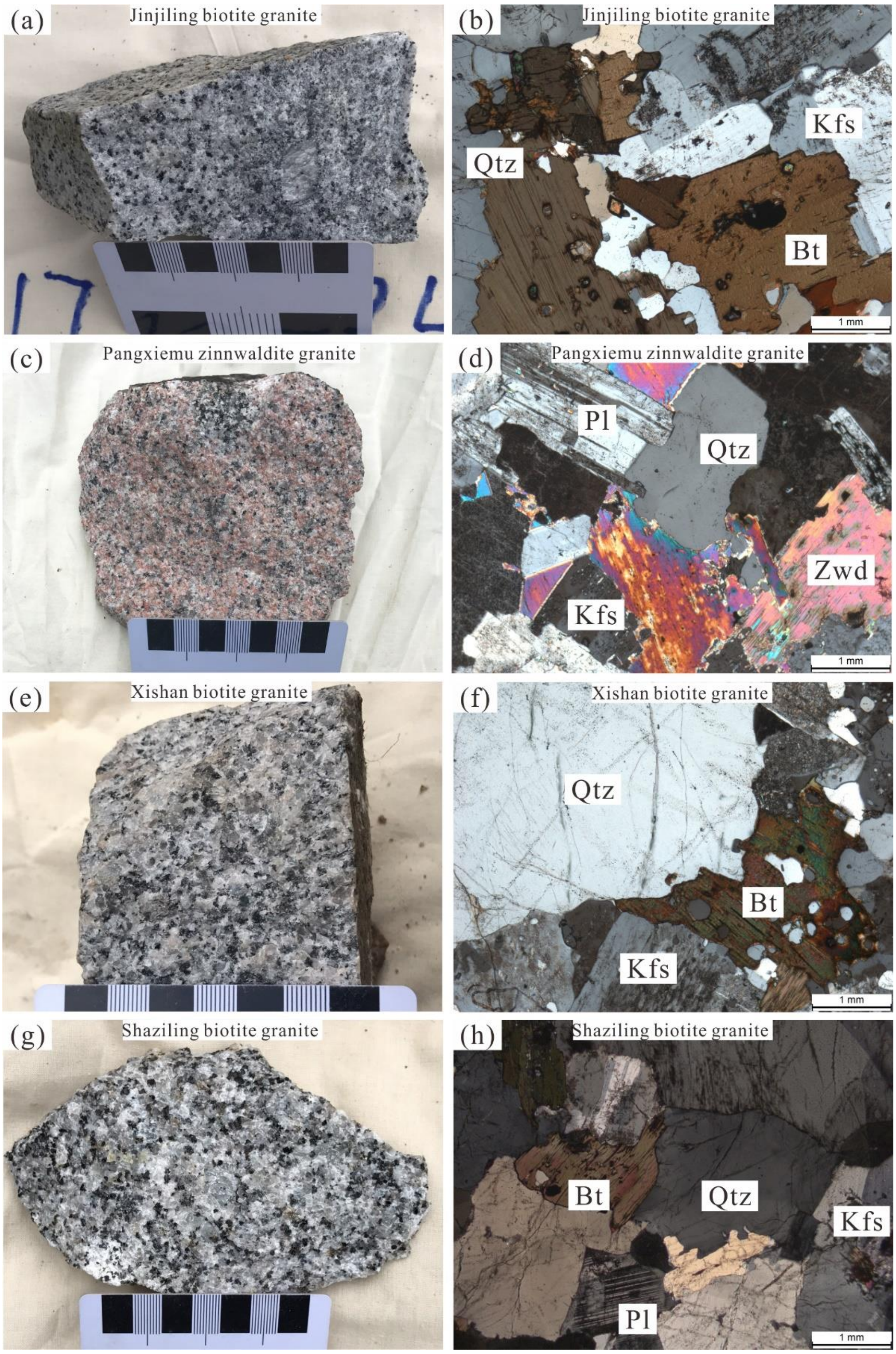

Figure 4. *Cont.*

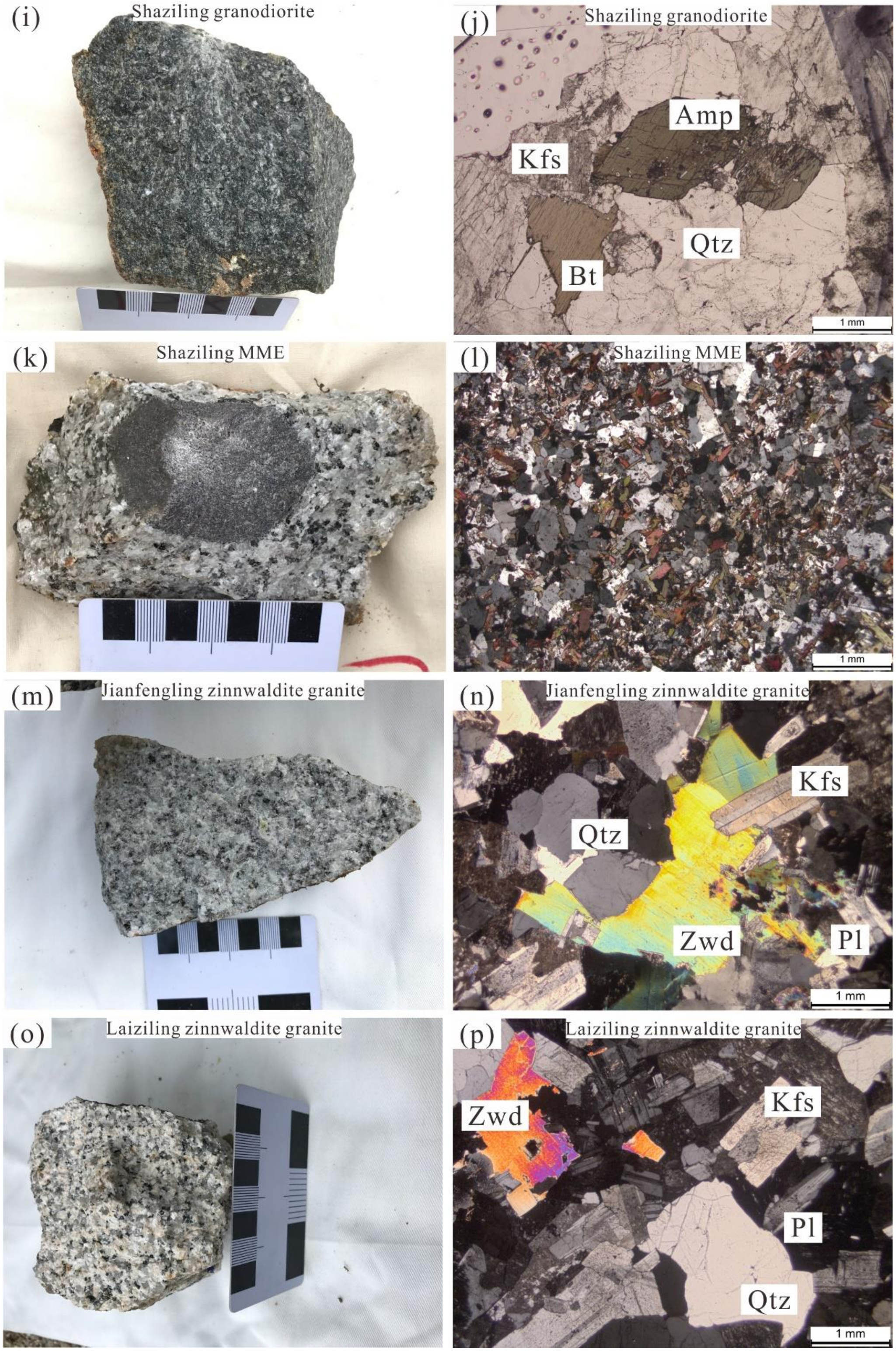

Figure 4. Hand specimens and photomicrographs of the Jiuyishan and Xianghualing granites. (**a**,**c**,**e**,**g**,**i**,**k**,**m**,**o**): Hand specimen of the Jinjiling biotite granite, Pangxiemu zinnwaldite granite, Xishan biotite granite, Shaziling biotite granite, Shaziling granodiorite, Shazling MME, Jianfengling zinnwaldite granite and Laiziling zinnwaldite granite, respectively. (**b**,**d**,**f**,**h**,**j**,**l**,**n**,**p**): Photomicrograph of the above lithologies. (**j**) is under plane-polarized light while (**b**,**d**,**f**,**h**,**l**,**n**,**p**) are under cross-polarized lights. Abbreviations: Amp—amphibole; Bt—biotite; Kfs—K-feldspar; Pl—plagioclase; Qtz—quartz; Zwd—zinnwaldite.

The Pangxiemu unit is composed of fine-to-medium-grained zinnwaldite granite with particle sizes of approximately 0.5–3 mm (Figure 4c). The samples of the Pangxiemu zinnwaldite granite are massive and light-pink-to-whitish colored, consisting of quartz (35%–40%), plagioclase (15%–20%), K-feldspar (30%–35%) and zinnwaldite (~5%), with accessory minerals of zircon and ilmenite (Figure 4d).

The Xishan unit is a volcanic-intrusive complex composed of granites, subvolcanic and volcanic rocks. The samples of the Xishan granites are mainly composed of medium-to-coarse-grained biotite granites with particle sizes of approximately 5–12 mm, and they are massive and light-gray-to-whitish colored, with porphyritic textures (Figure 4e). The groundmass is composed of quartz (30%–35%), plagioclase (20%–25%), K-feldspar (30%–35%) and biotite (~5%), with accessory minerals of zircon, titanite and ilmenite (Figure 4f). The phenocrysts are mainly composed of plagioclase and K-feldspar, with particle sizes of approximately 10–30 mm.

The Shaziling unit comprises medium-to-fine-grained granodiorite and biotite granite, with abundant MMEs developed inside the host rocks of biotite granite. The samples of the Shaziling biotite granites are massive and light-gray-to-whitish colored (Figure 4g), with particle sizes of approximately 1–5 mm, consisting of quartz (25%–30%), plagioclase (20%–25%), K-feldspar (30%–35%), biotite (~10%) and minor amphibole. The accessory minerals are mainly zircon, apatite, titanite and ilmenite (Figure 4h). The samples of the Shaziling granodiorite are massive and light-gray-to-black colored (Figure 4i), with particle sizes of approximately 0.5–3 mm, consisting of quartz (20%–25%), plagioclase (20%–25%), K-feldspar (30%–35%), biotite (~10%) and amphibole (~5%) (Figure 4j). The MMEs are black colored and fine-grained (Figure 4k), with particle size of approximately 0.1–0.5 mm, consisting of mainly quartz, amphibole, feldspar and biotite (Figure 4l).

The Jianfengling and Laiziling intrusive stocks show vertical zonation of biotite granite at the bottom, zinnwaldite granite in the middle, and topaz granite at the top. However, in this study, only zinnwaldite granite samples were collected to perform a petrographic study. The samples of the Jianfengling granites are fine-grained zinnwaldite granite with particle sizes of approximately 0.5–2 mm; they are massive and light-gray-to-whitish colored (Figure 4m), consisting of quartz (35%–40%), plagioclase (15%–20%), K-feldspar (30%–35%) and zinnwaldite (~5%), with accessory minerals of zircon and ilmenite (Figure 4n).

The samples of the Laiziling granites are fine-grained zinnwaldite granite with particle sizes of approximately 0.5–2 mm; they are massive and light-gray-to-whitish colored (Figure 4o), consisting of quartz (35%–40%), plagioclase (20%–25%), K-feldspar (25%–30%) and zinnwaldite (~5%), with accessory minerals of zircon and ilmenite (Figure 4p).

3. Analytical Methods

3.1. Zircon U-Pb Dating

Before the analysis, the zircon grains from the samples were separated using conventional magnetic and heavy liquid techniques. Subsequently, they were hand-picked under a binocular microscope at Langfang Integrity Geological Services Co., Ltd., Langfang, China. Next, they were mounted into epoxy resin blocks and polished to obtain flat surfaces. The cathodoluminescence (CL) imaging technique was used to visualize the internal structures of individual zircon grains with a scanning electron microscope (SEM), which was housed at Yujing Science and Technology Services Co., Ltd., Chongqing, China.

U-Pb geochronology of zircon was conducted by LA-ICP-MS at FocuMS Technology Co., Ltd., Nanjing, China. The Teledyne Cetac Technologies Analyte Excite laser-ablation system (Bozeman, MT, USA) and Agilent Technologies 7700× quadrupole ICP-MS (Hachioji, Tokyo, Japan) were combined for the experiments. The 193-nm ArF excimer laser, which was homogenized via a set of beam delivery systems, was focused on the zircon surface with a fluence of 6.0 J/cm^2. The ablation protocol employed a spot diameter of 35 μm at an 8-Hz repetition rate for 40 s (equating to 320 pulses). Helium was applied as a carrier gas to efficiently transport the aerosol to ICP-MS. Zircon 91500 was used as an external standard to correct instrumental mass discrimination and elemental fractionation during the ablation. Zircon GJ-1 was treated as a quality control for geochronology. The lead abundance of zircon was externally calibrated against NIST SRM 610 with Si as the internal standard, while Zr was the internal standard for other trace elements [47,48]. Raw data reductions were performed offline using ICPMSDataCal software [47,49].

3.2. Whole-Rock Major and Trace Element Analysis

The whole-rock major and trace element compositions were analyzed at ALS Chemex, Guangzhou, China. The samples were crushed in a sample crusher to pass through a 200-mm mesh before major element contents were measured using a Panalytical Axios Max X-ray fluorescence (XRF) instrument with an analytical accuracy of between 1%–5%. Trace element compositions were measured using ICP-MS (Perkin Elmer Elan 9000) with an analytical accuracy greater than 5%.

3.3. Zircon Lu-Hf Isotope Analysis

Hafnium isotopic ratios of zircon were determined by LA-MC-ICP-MS at FocuMS Technology Co., Ltd., Nanjing, China. The Teledyne Cetac Technologies Analyte Excite laser-ablation system (Bozeman, MT, USA) and Nu Instruments Nu Plasma II MC-ICP-MS (Wrexham, Wales, UK) were combined for the experiments. The 193-nm ArF excimer laser, which was homogenized via a set of beam delivery systems, was focused on the zircon surface with fluence of 6.0 J/cm^2. The ablation protocol employed a spot diameter of 50 μm at an 8-Hz repetition rate for 40 s (equating to 320 pulses). Helium was applied as a carrier gas to efficiently transport the aerosol to MC-ICP-MS. Two standard zircons (GJ-1 and 91500) were treated as the quality controls for every ten unknown samples.

3.4. Whole-Rock Nd-Pb Isotope Analysis

High-precision isotopic (Nd, Pb) measurements were carried out at FocuMS Technology Co., Ltd., Nanjing, China. Geological rock powders were decomposed using high-pressure PTFE bombs. Neodymium and lead were all purified from the same digestion solution via two steps of column chemistry. The first exchange column combined with BioRad AG50 W×8 and Sr Spec resin was used to separate Sr, REE and Pb from the sample matrix. Neodymium was separated from the other REEs on the second column with Ln Spec-coated Teflon powder. The Nd- and Pb-bearing eluates were dried down and redissolved in 1.0 mL of 2 wt.% HNO_3. Small aliquots of each elution were analyzed using Agilent Technologies 7700× quadrupole ICP-MS (Hachioji, Tokyo, Japan) to determine the exact contents of available Nd and Pb. A diluted solution (50 ppb Nd and 40 ppb Pb doped with 10 ppb Tl) was introduced into Nu Instruments' Nu Plasma II MC-ICP-MS (Wrexham, Wales, UK) via the Teledyne Cetac Technologies Aridus II desolvating nebulizer system (Omaha, NE, USA). Raw data of isotopic ratios were corrected for mass fractionation by normalizing to $^{146}Nd/^{144}Nd$ = 0.7219 for Nd and $^{205}Tl/^{203}Tl$ = 2.3885 for Pb using the exponential law. International isotopic standards (JNdi-1 for Nd and NIST SRM 981 for Pb) were periodically analyzed to correct for instrumental drift. Geochemical reference materials of USGS BCR-2, BHVO-2, AVG-2 and RGM-2 were treated as the quality controls.

4. Analytical Results

4.1. Zircon U-Pb Dating

The analytical results of zircon LA-ICP-MS U-Pb dating are presented in Supplementary Table S1, and CL images of representative zircons are shown in Figure 5. Zircons from four units of the Jiuyishan complex which were picked for dating are transparent and colorless and show distinct oscillatory zoning, indicating that they are magmatic zircons [50,51]. A total of 38 zircons from the Jinjiling granite are concordant (>90%), and they yielded a weighted mean $^{206}Pb/^{238}U$ age of 152.5 ± 0.7 Ma (MSWD = 0.95) (Figure 6). A total of 15 zircons from the Pangxiemu granite yielded a weighted mean $^{206}Pb/^{238}U$ age of 153.8 ± 1.5 Ma (MSWD = 1.6) (Figure 6). A total of 20 zircons from the Shaziling granite yielded a weighted mean $^{206}Pb/^{238}U$ age of 152.9 ± 1.0 Ma (MSWD = 0.039) (Figure 6).

A total of 36 zircons from the Xishan granite yielded a weighted mean $^{206}Pb/^{238}U$ age of 153.0 ± 0.7 Ma (MSWD = 0.014) (Figure 6). A total of 19 zircons from the Shaziling MMEs yielded a weighted mean $^{206}Pb/^{238}U$ age of 152.1 ± 1.1 Ma (MSWD = 0.31) (Figure 6). A total of 18 zircons from the Pangxiemu dolerite yielded a weighted mean $^{206}Pb/^{238}U$ age of 153.1 ± 1.0 Ma (MSWD = 0.78) (Figure 6).

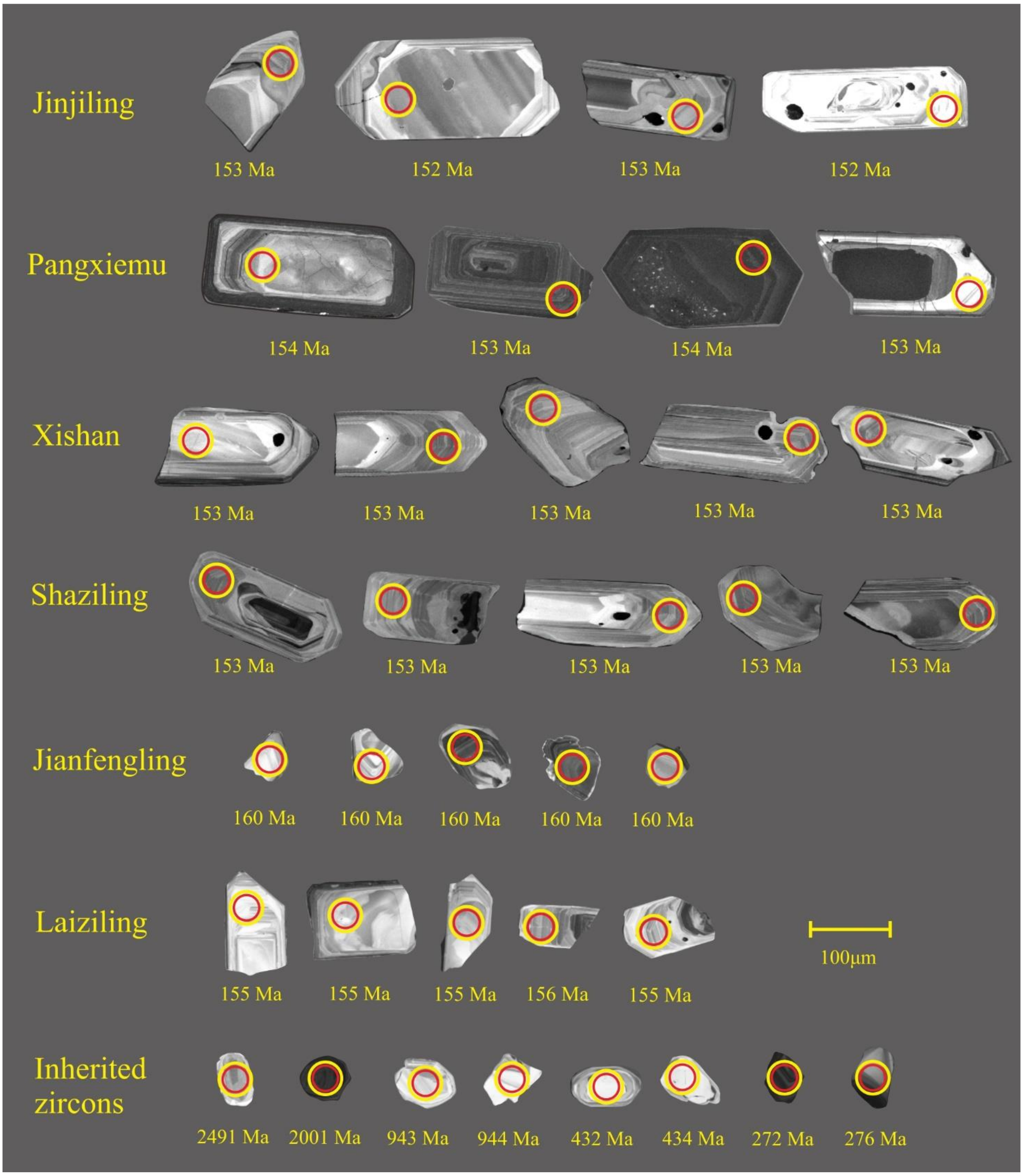

Figure 5. Representative zircon cathodoluminescence (CL) images. The solid red (diameter = 35 μm) and yellow (diameter = 44 μm) circles on the zircon CL images indicate the locations of U-Pb age and Hf isotope sites, respectively.

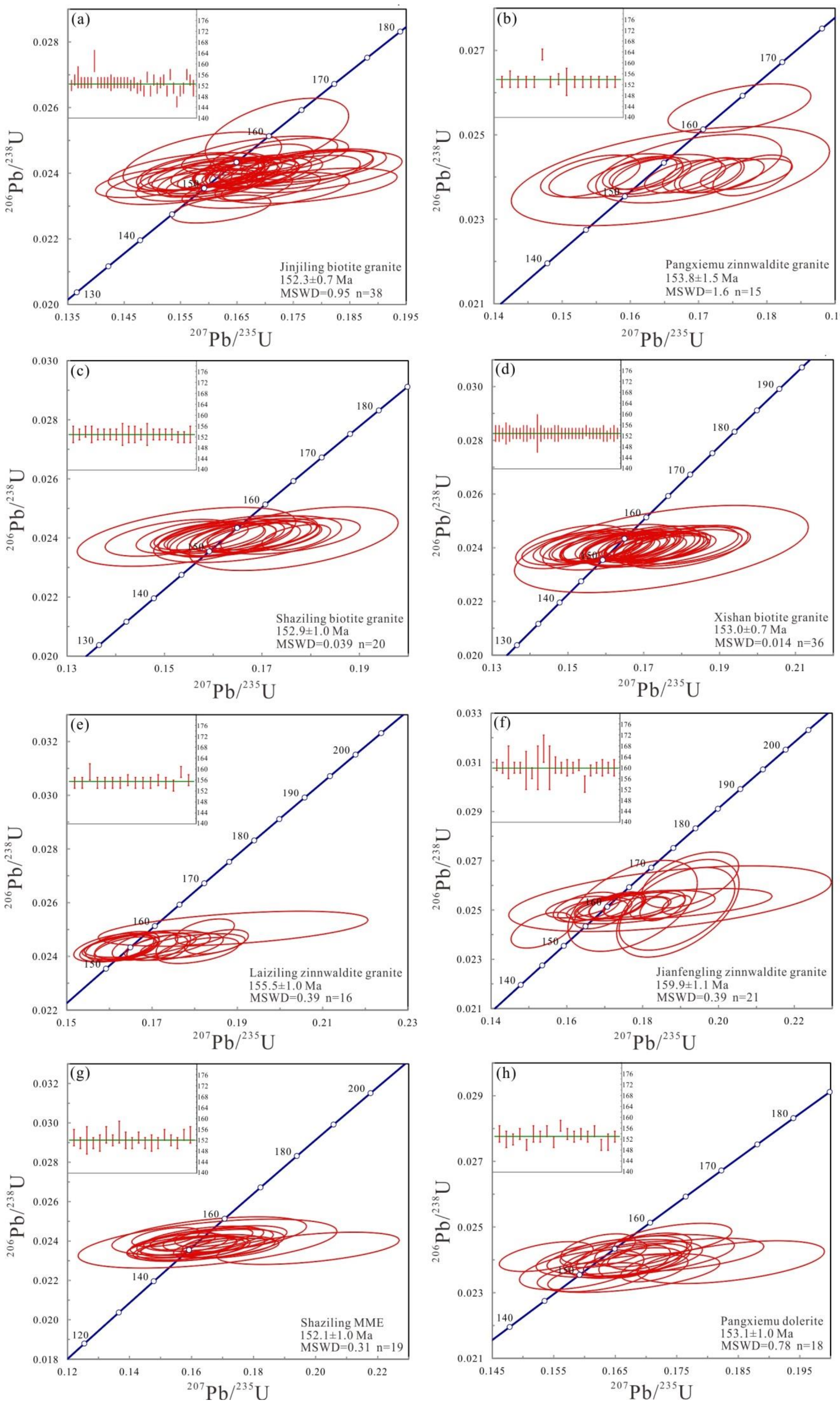

Figure 6. Zircon U-Pb concordia diagrams and weighted mean age diagrams. (**a**) Jinjiling biotite granite; (**b**) Pangxiemu zinnwaldite granite; (**c**) Shaziling biotite granite; (**d**) Xishan biotite granite; (**e**) Laiziling zinnwaldite granite; (**f**) Jianfengling zinnwaldite granite; (**g**) Shaziling MME; (**h**) Pangxiemu dolerite.

Zircons from the Laiziling and Jianfengling stocks which were picked for dating are transparent and colorless and show distinct oscillatory zoning, but some grains harbor dark areas, indicating that they are magmatic zircons but experienced different levels of metamictization. A total of 22 zircons from the Jianfengling granite yield a weighted mean $^{206}Pb/^{238}U$ age of 159.9 ± 1.1 Ma (MSWD = 0.39) (Figure 6). A total of 16 zircons from the Laiziling granite yield a weighted mean $^{206}Pb/^{238}U$ age of 155.5 ± 1.0 Ma (MSWD = 0.39) (Figure 6). Moreover, inherited zircons are abundant in the Laiziling and Jianfengling granites, the zircon U-Pb dating results of which are presented in Supplementary Table S2. Most of these inherited zircons have good psephicity, bright CL images and concordant ages ranging from 2500 Ma to 182 Ma (Figure 5).

4.2. Whole-Rock Major Elements

The whole-rock major and trace element analytical results are presented in Supplementary Table S3. Samples of the Jinjiling biotite granites (n = 19), Pangxiemu zinnwaldite granites (n = 14), Shaziling granodiorites and biotite granites (n = 12) and Xishan biotite granites (n = 19) have moderate-to-high SiO_2, Na_2O and K_2O contents; on the TAS diagram, they all plot in the granite field (Figure 7a). They have moderate A/CNK values, belonging to the metaluminoustoweakly peraluminous series (Figure 7b); they have high $Na_2O + K_2O\text{-}CaO$ contents and $FeO^T/(FeO^T + MgO)$ values and mostly plot in the calc-alkalic and ferroan series, respectively (Figure 7c,d).

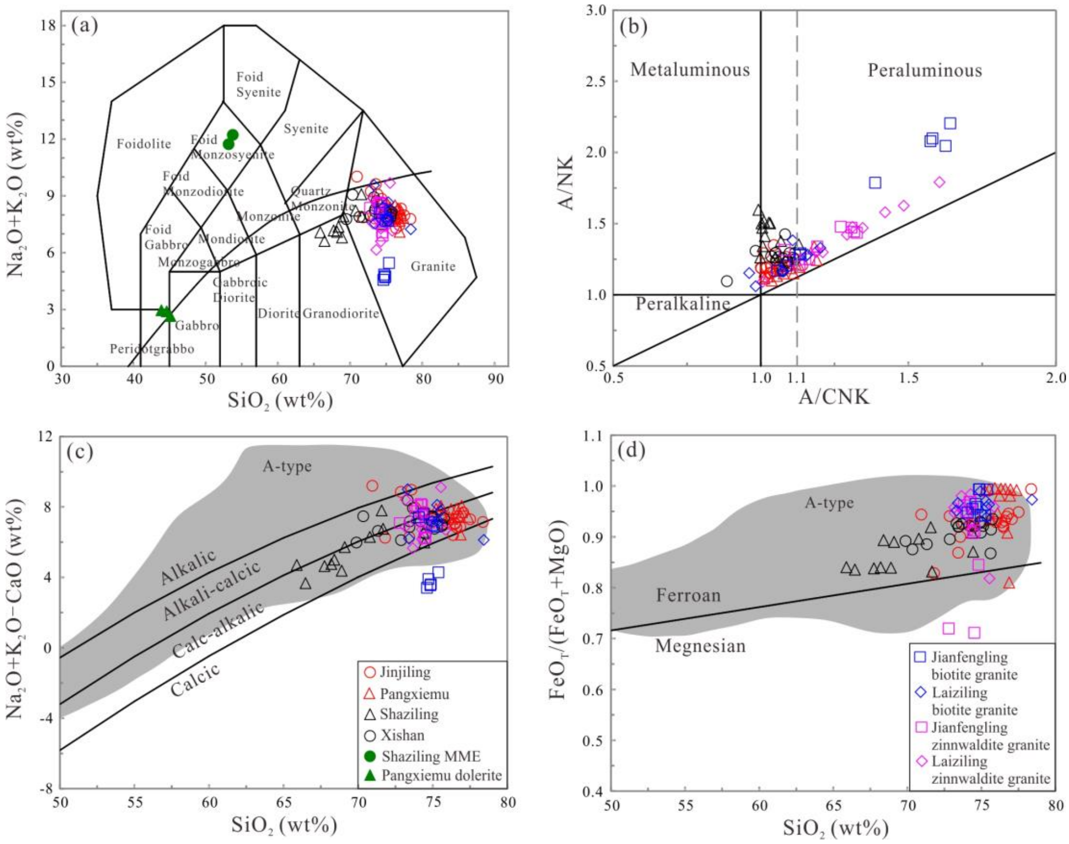

Figure 7. (**a**) TAS diagram (after Middlemost, [52]); (**b**) A/NK vs. A/CNK diagram (after Maniar and Piccoli, [53]); (**c**) SiO_2 vs. $Na_2O + K_2O\text{-}CaO$ diagram (after Frost et al. [54]); (**d**) SiO_2 vs. $FeO^T/(FeO^T + MgO)$ diagram (after Frost et al. [54]).

Samples of the Laiziling and Jianfengling biotite and zinnwaldite granites have high SiO_2, Na_2O and K_2O contents. On the TAS diagram, they all plot in the granite field (Figure 7a). They have high A/CNK values and are weakly-to-strongly peraluminous

(Figure 7b); they have high Na_2O + K_2O-CaO contents and $FeO^T/(FeO^T + MgO)$ values and mostly plot in the calc-alkalic and ferroan series, respectively (Figure 7c,d).

Moreover, samples from the Shaziling MMEs and Pangxiemu dolerite are also introduced here. The Shaziling MMEs have low SiO_2, Na_2O and K_2O contents; on the TAS diagram, they all plot in the foid monzosyenite field (Figure 7a). The Pangxiemu dolerite has low SiO_2, Na_2O and K_2O contents; on the TAS diagram, they all plot in the peridotegabbro field (Figure 7a).

4.3. Whole-Rock Trace Elements

The Jinjiling, Shazilig and Xishan granites have similar trace element distribution patterns: they show moderate enrichment in Rb, Th, U, Ta, Nb, Zr and Hf and depletion in Ba, Sr, P and Ti (Figure 8a,e,g). They also show similar rare-earth element (REE) distribution patterns of a right-dipping shape (Figure 8b,f,h). They have strong LREE/HREE fractionation and moderate negative Eu anomalies. The Pangxiemu, Jianfengling and Laiziling granites also have similar trace element distribution patterns: they show extreme enrichments in Rb, Th, U, Ta, Nb, Zr and Hf and depletions in Ba, Sr, P and Ti (Figure 8c,k,m). They show similar rare-earth element (REE) distribution patterns that are flat V-shaped (Figure 8d,l,n). They have slight LREE/HREE fractionation and extreme negative Eu anomalies.

The Shaziling MMEs have trace element distribution patterns that show slight enrichment in Rb and U and depletion in Ba, Nb, Ta, Sr, P and Ti (Figure 8i). They show rare-earth element (REE) distribution patterns of a right-dipping shape (Figure 8j). They have strong LREE/HREE fractionation and weak Eu anomalies. The Pangxiemu dolerite has trace element distribution patterns that show slight enrichment in Rb and Th and depletion in Ba and Sr (Figure 8i). They show rare-earth element (REE) distribution patterns of a right-dipping shape (Figure 8j). They have strong LREE/HREE fractionation and nearly no Eu anomalies.

4.4. Zircon Lu-Hf Isotopes

The LA-MC-ICP-MS analytical results of the zircon Lu-Hf isotope compositions are presented in Supplementary Table S4 and also shown in Figure 9. Zircons from the Jinjiling granites have εHf(t) values ranging from −5.8 to −2.2, with an average of −4.2 (n = 10); the two-stage model ages (T_{DM2}) range from 1338 to 1563 Ma, with an average of 1467 Ma. Zircons from the Pangxiemu granites have εHf(t) values ranging from −5.0 to −2.5, with an average of −3.7 (n = 10); the two-stage model ages (T_{DM2}) range from 1360 to 1516 Ma, with an average of 1436 Ma. Zircons from the Shaziling granites have εHf(t) values ranging from −7.5 to −4.7, with an average of −6.2 (n = 10); the two-stage model ages (T_{DM2}) range from 1498 to 1672 Ma, with an average of 1588 Ma. Zircons from the Xishan granites have εHf(t) values ranging from −9.1 to −4.0, with an average of −6.0 (n = 20); the two-stage model ages (T_{DM2}) range from 1453 to 1770 Ma, with an average of 1580 Ma. Zircons from the Shaziling MMEs have εHf(t) values ranging from −14.2 to 4.8, with an average of −3.9 (n = 19); they have two-stage model ages (T_{DM2}) ranging from 894 to 2097 Ma, with an average of 1448 Ma.

Zircons from the Laiziling granites have εHf(t) values ranging from −7.6 to −2.7, with an average of −4.5 (n = 16); the two-stage model ages (T_{DM2}) range from 1423 to 1653 Ma, with an average of 1484 Ma. The zircons from the Jianfengling granites have εHf(t) values ranging from −7.1 to −3.8, with an average of −4.9 (n = 15); the two-stage model ages (T_{DM2}) range from 1370 to 1677 Ma, with an average of 1514 Ma.

4.5. Whole-Rock Sr-Nd-Pb Isotopes

The analytical results and referenced data of whole-rock Sr-Nd isotope compositions are presented in Supplementary Table S5 and also shown in Figure 9. The analytical results of whole-rock Pb isotopic compositions of the Jianfengling and Laiziling granites are presented in Supplementary Table S6 and also shown in Figure 9.

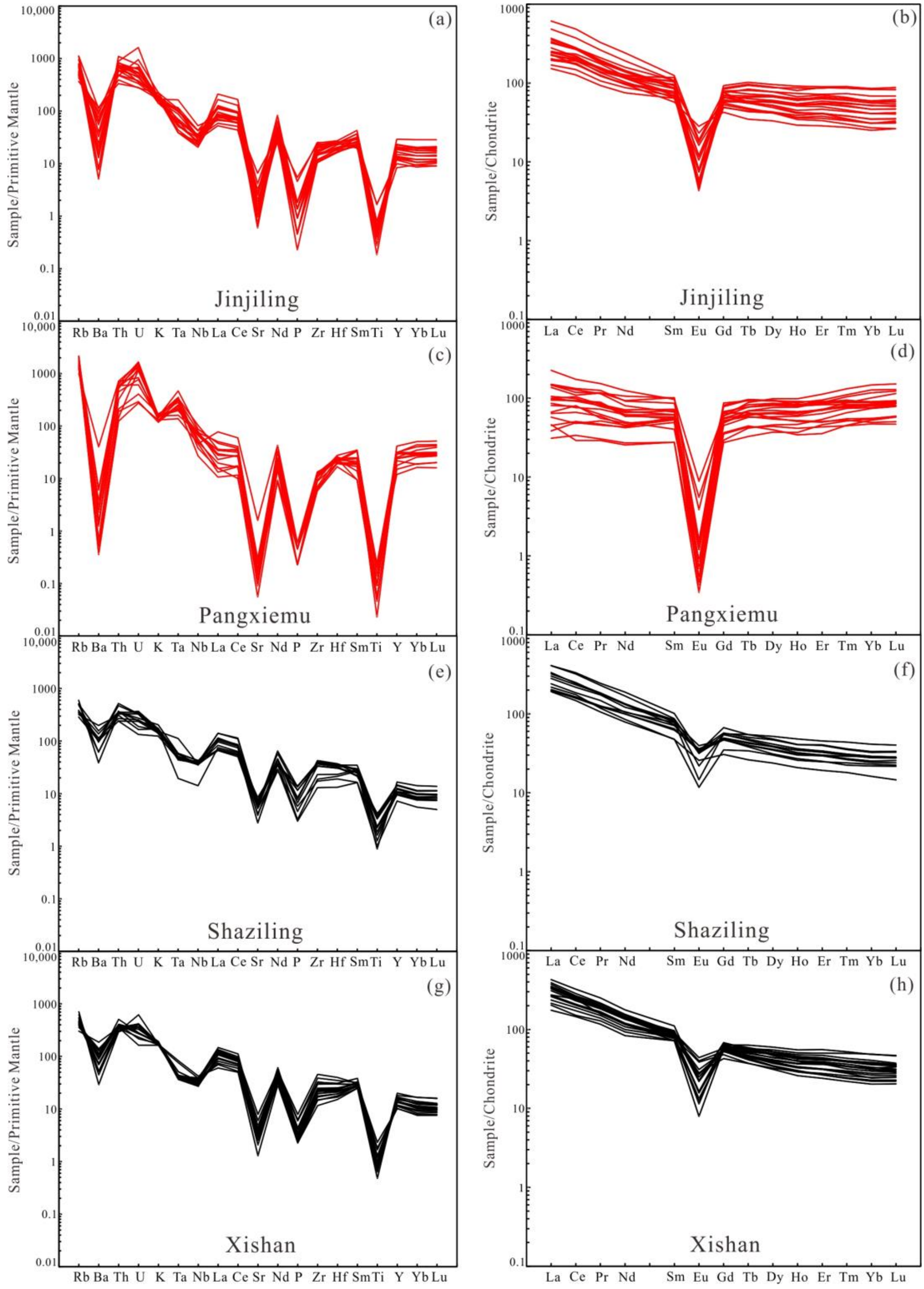

Figure 8. *Cont*.

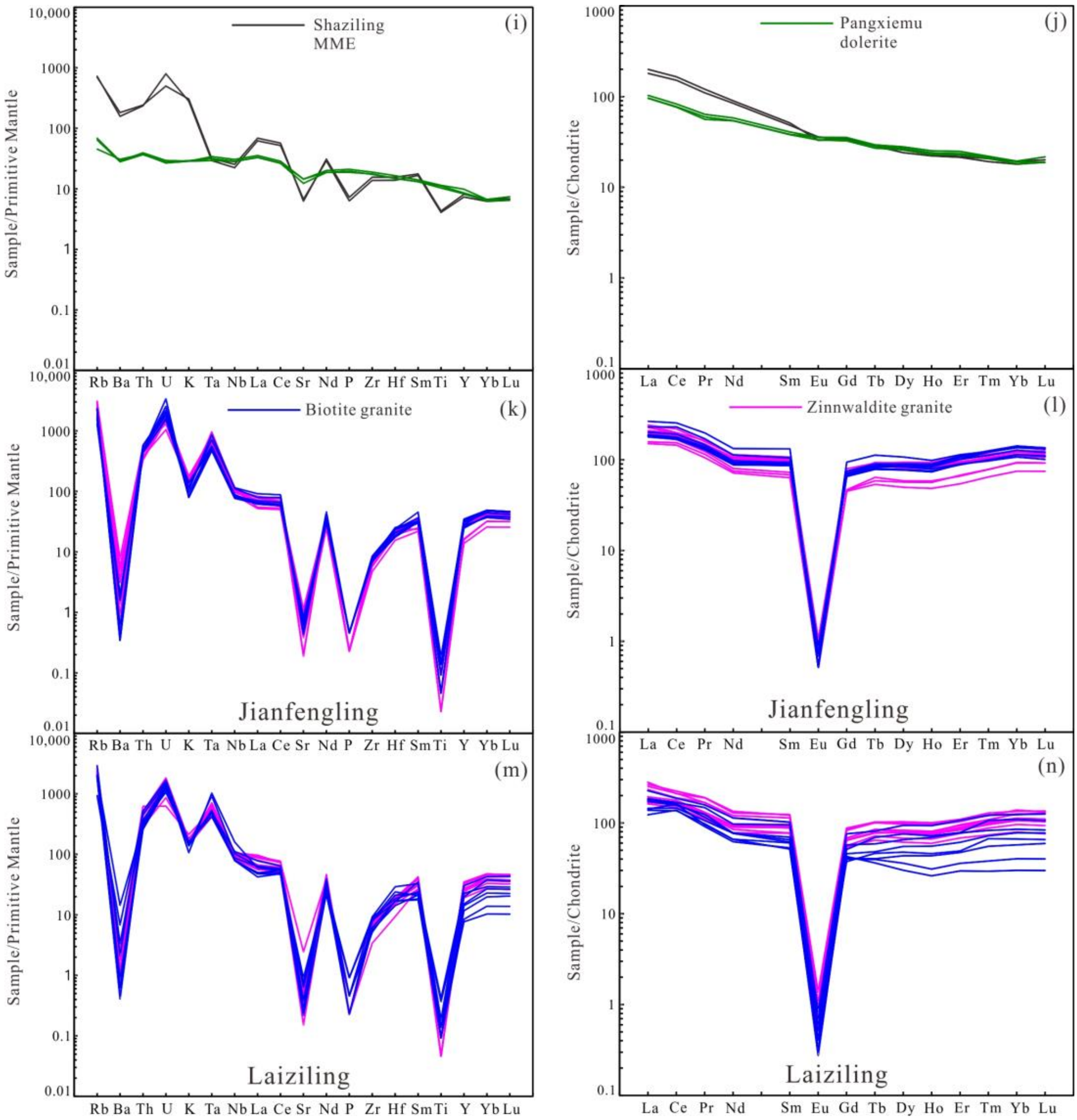

Figure 8. Primitive mantle-normalized trace element spider diagrams and Chondrite-normalized rare-earth element distribution pattern diagrams. (**a**,**c**,**e**,**g**,**i**,**k**,**m**): Primitive mantle-normalized trace element spider diagrams of the Jinjiling granites, Pangxiemu granites, Shaziling granites, Xishan granites, Shaziling MMEs (Pangxiemu dolerites), Jianfengling biotite granites (zinnwaldite granites) and Laiziling biotite granites (zinnwaldite granites), respectively. (**b**,**d**,**f**,**h**,**j**,**l**,**n**): Chondrite-normalized rare-earth element distribution pattern diagrams of the above lithologies. The Chondrite-normalized and primitive mantle-normalized values are from Sun and McDonough [55].

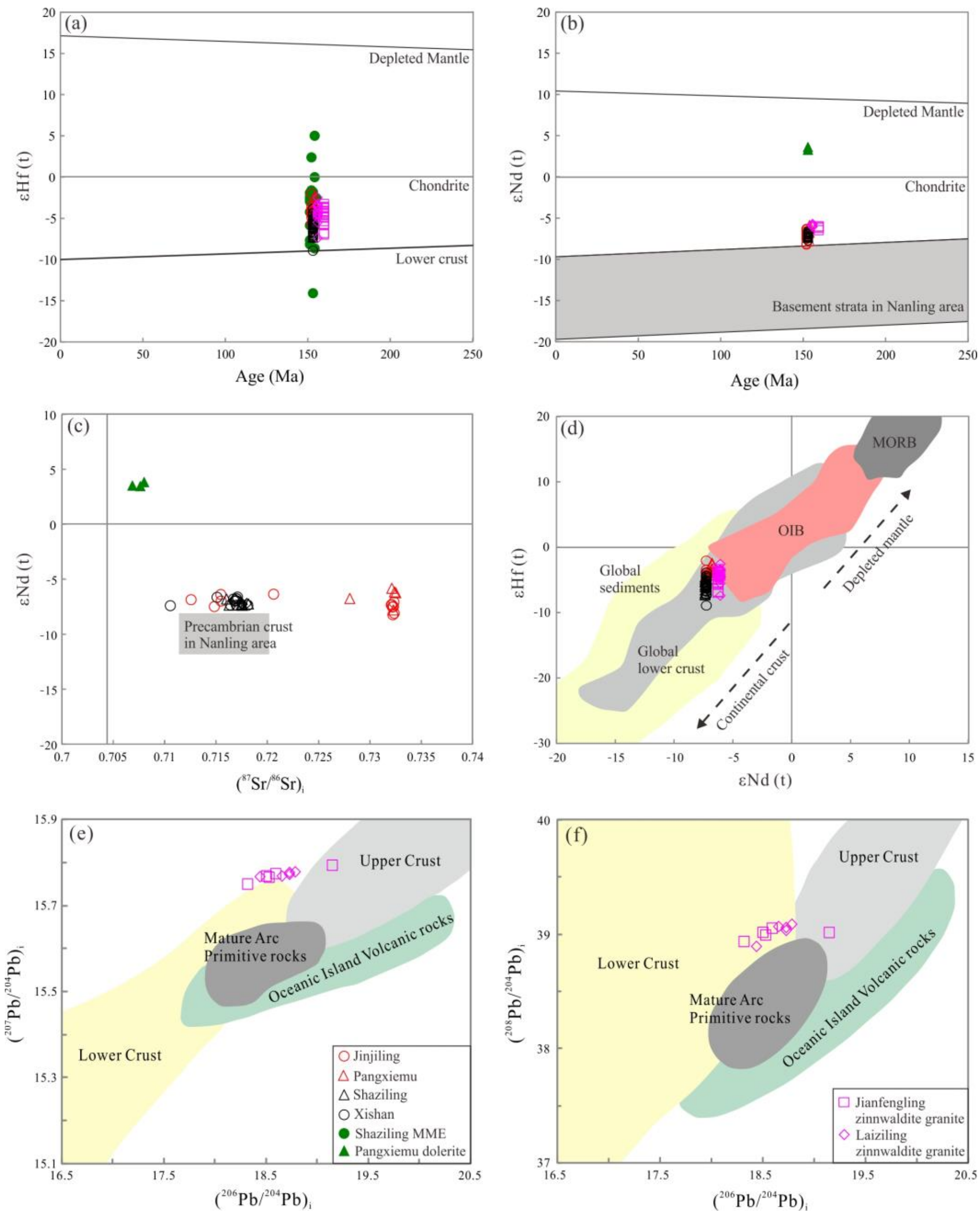

Figure 9. (**a**) Zircon ages vs. εHf(t) diagram; (**b**) zircon ages vs. whole-rock εNd(t) diagram (after Shu et al. [12]); (**c**) whole-rock $(^{87}Sr/^{86}Sr)_i$ vs. εNd(t) diagram (after Zhao et al. [56]); (**d**) whole-rock εNd(t) vs. zircon εHf(t) diagram (after Zhu et al. [57]); (**e**) whole-rock $(^{206}Pb/^{204}Pb)_i$ vs. $(^{207}Pb/^{204}Pb)_i$ diagram (after Zhu et al. [57]); (**f**) whole-rock $(^{206}Pb/^{204}Pb)_i$ vs. $(^{208}Pb/^{204}Pb)_i$ diagram (after Zhu et al. [57]).

The Jinjiling granites have εNd(t) values ranging from −8.2 to −6.3, with an average of −7.1 (n = 17); the two-stage model ages (T_{DM2}) range from 1389 to 1556 Ma, with an average of 1472 Ma; and they have $(^{87}Sr/^{86}Sr)_i$ values ranging from 0.7126 to 0.7324. The Pangxiemu granites have εNd(t) values ranging from −7.8 to −5.8, with an average of −6.6 (n = 3); the two-stage model ages (T_{DM2}) range from 1084 to 1513 Ma, with an average of 1327 Ma; and they have $(^{87}Sr/^{86}Sr)_i$ values ranging from 0.7280 to 0.7325. The Shaziling granites have εNd(t) values ranging from −7.4 to −6.8, with an average of −7.2 (n = 8); the two-stage model ages (T_{DM2}) range from 1542 to 1546 Ma, with an average of 1533 Ma; and they have $(^{87}Sr/^{86}Sr)_i$ values ranging from 0.7160 to 0.7182. The Xishan granites have εNd(t) values ranging from −7.7 to −6.6, with an average of −7.1 (n = 17); the two-stage model ages (T_{DM2}) range from 1486 to 1571 Ma, with an average of 1523 Ma; and they have $(^{87}Sr/^{86}Sr)_i$ values ranging from 0.7106 to 0.7181. The Pangxiemu dolerite has εNd(t) values ranging from 3.4 to 3.8, with an average of 3.5 (n = 3); the one-stage model ages (T_{DM}) range from 776 to 815 Ma, with an average of 799 Ma; and they have $(^{87}Sr/^{86}Sr)_i$ values ranging from 0.7068 to 0.7080.

The Laiziling granites have εNd(t) values ranging from −6.1 to −5.7, with an average of −5.9 (n = 5); the two-stage model ages (T_{DM2}) range from 1409 to 1439 Ma, with an average of 1422 Ma; and they have $(^{206}Pb/^{204}Pb)_i$, $(^{207}Pb/^{204}Pb)_i$, and $(^{208}Pb/^{204}Pb)_i$ ratios ranging from 18.317 to 19.149, 15.747 to 15.791 and 38.927 to 39.044, respectively. The Jianfengling granites have εNd(t) values ranging from −6.5 to −6.0, with an average of −6.1 (n = 5); the two-stage model ages (T_{DM2}) range from 1437 to 1474 Ma, with an average of 1448 Ma; and they have $(^{206}Pb/^{204}Pb)_i$, $(^{207}Pb/^{204}Pb)_i$, and $(^{208}Pb/^{204}Pb)_i$ ratios ranging from 18.439 to 18.785, 15.764 to 15.775 and 38.885 to 39.078, respectively.

5. Discussion

5.1. Geochronology and Genetic Type

The zircon U-Pb dating results show that the Jinjiling (152.3 ± 0.7 Ma), Pangxiemu (153.8 ± 1.5 Ma), Shaziling (152.9 ± 1.0 Ma) and Xishan (153.0 ± 0.7 Ma) units of the Jiuyishan complex massif have indistinguishable ages between 154 Ma and 152 Ma (Figure 6), which are consistent within the error range. In addition, the zircon U-Pb dating of the Shaziling MMEs and the Pangxiemu dolerite dike also yielded nearly the same ages of 152.1 ± 1.1 Ma [35] and 153.1 ± 0.9 Ma [37], respectively. Adjacent mafic rocks and MMEs strongly support the injection of mantle-derived magma, and the indistinguishable ages between the dolerite, MMEs and Shaziling granodiorite indicate the recharge of magma chambers, which commonly occurred in large complex massifs with crystal mush systems [58]. In comparison, the Laiziling and Jianfengling intrusive stocks show different emplacement ages. The zircon U-Pb dating result of the Laiziling stock yields an age of 155.5 ± 1.0 Ma, which is slightly earlier than the ages of the Jiuyishan complex massif, which were between 154 Ma and 152 Ma. However, the zircon U-Pb dating result of the Jianfengling stock yielded ages of 159.9 ± 1.1 Ma, which is nearly 5 Myr earlier than the Laiziling stock. Although these two stocks have similar geochemical and isotopic compositions, implying they have the same sources, the age gaps between them suggest two stages of emplacement.

Although the definition of A-type granite has been broadened, compared to I- and S-type granites, four units of the Jiuyishan complex and Jianfengling and Laiziling stocks show common features: high SiO_2 and $Na_2O + K_2O$ contents and FeO^T/MgO ratios but low CaO, MgO and P_2O_5 contents, demonstrating A-type features [8]. Moreover, the enrichment in HFSEs, Ga, Rb, Th and U and the depletion in Ba, Sr, Ti, P and Eu contents are also geochemical features of A-type granites, regardless of the crystal fractionation process [7,59]. In the diagrams of 10,000 Ga/Al vs. $(K_2O + Na_2O)/Ca$, Zr + Nb + Ce + Y vs. FeO^T/MgO (Figure 10a,b), SiO_2 vs. $Na_2O + K_2O$-CaO and SiO_2 vs. $FeO^T/(FeO^T + MgO)$ (Figure 10c,d), four units and two stocks all plot in the A-type field, and they plot in the A_2-type field in the diagrams of Nb-Y-Ce and Nb-Y-3 Ga (Figure 10c,d), indicating the formation in an intraplate extensional environment. Petrography shows that four units and two stocks have abundant alkali feldspars [10,42,44], which is an important mineralogical indicator of A-type granite [5]. The Jinjiling (763–834 °C), Shaziling (782–878 °C) and Xishan (775–918 °C) granites have relatively high formation temperatures—estimated using the zircon saturation geothermometer—compared to the highly evolved Pangxiemu (702–779 °C), Jianfengling (718–773 °C) and Laiziling (686–770 °C) granites, which is also an important characteristic of A-type granite [60,61]. In summary, four units and two stocks all have A-type affinities with ages between 160 Ma and 150 Ma.

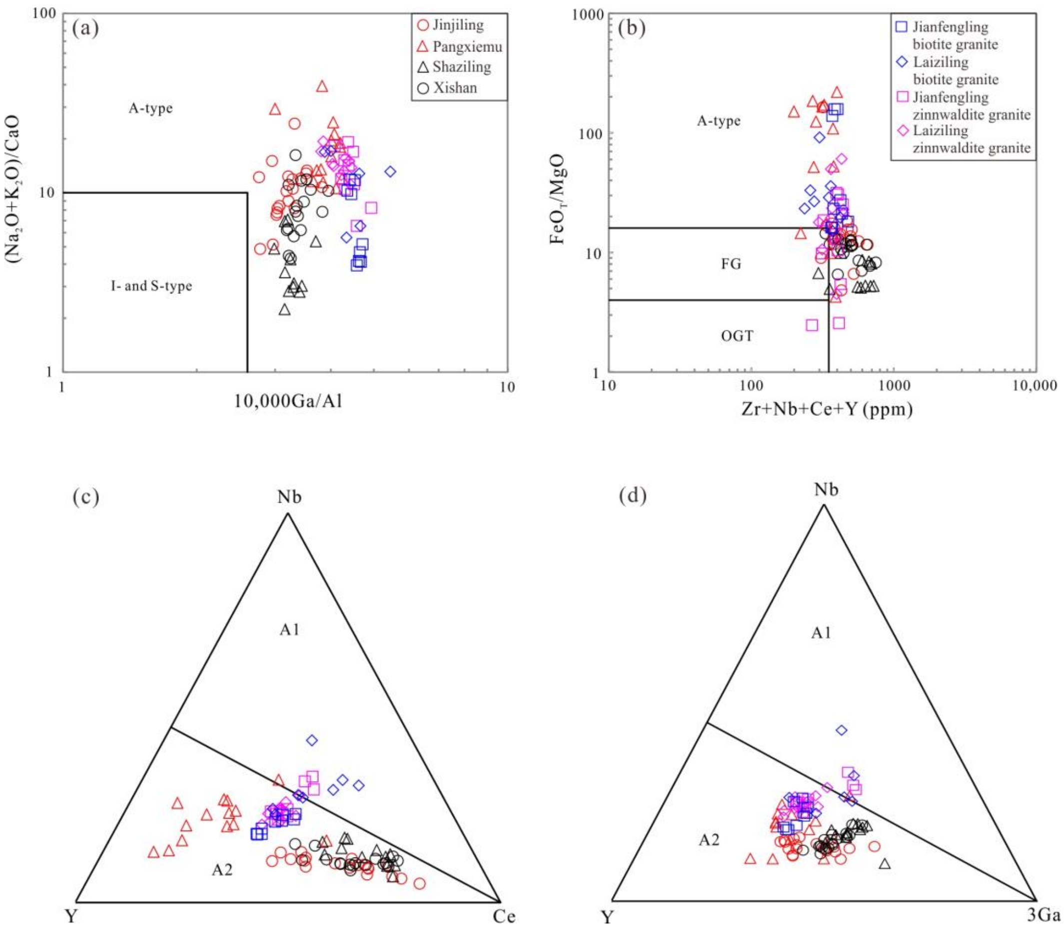

Figure 10. (**a**) 10,000 Ga/Al vs. (K_2O + Na_2O)/Ca diagram (after Whalen et al. [62]); (**b**) Zr + Nb + Ce + Y vs. FeO^T/MgO diagram (after Whalen et al. [62]); (**c**) Nb-Y-Ce diagram (after Eby, [63]); (**d**) Nb-Y-3 Ga diagram (after Eby, [63]).

5.2. Petrogenesis of the Jiuyishan Complex Massif

Four units of the Jiuyishan complex massif have consistent zircon U-Pb ages and obtained similar whole-rock εNd(t) values (−8.2 to −5.8) and zircon εHf(t) values (−7.5 to −2.2), indicating that they were formed from the same magmatic event with the same source region. However, their relatively narrow range of εNd(t) and εHf(t) values can preclude mixed magma of disparate end-members [64,65]. Four units have similar T_{DM2} ages of between 1338–1770 Ma, which suggests that they are recycled products of Mesoproterozoic and Paleoproterozoic crustal materials. However, their εNd(t) values are slightly higher than the basement strata of the Nanling Range (Figure 9b,c), while their εHf(t) values are also slightly higher than the zircons of the Nanling basement rocks. Thus, their source region could be linked to more juvenile crustal materials when compared to the Paleoproterozoic crustal basement. Previous studies suggest that A_2-type granites in an intraplate extensional environment possibly have lower crustal sources. Due to their high temperature, low pressure and oxygen fugacity, most A_2-type granites were formed by the partial melting of lower crustal granulitic metasedimentary or metaigneous rocks [2,36]. In this study, four units of the Jiuyishan complex have zircon εHf(t) values beyond the lower crustal evolution line in South China (Figure 9a), which are plotted in the global lower crust field in the εNd(t) vs. εHf(t) diagram (Figure 9d), demonstrating a lower crustal source region with the incorporation of more juvenile materials.

Although an interpretation of lower crustal granulitic protoliths has been proposed, few studies have illustrated the specific protoliths of these four units. Whole-rock geochemical compositions can be a significant indicator for tracing magma sources of the low-degree-evolved granites [33,66], while the highly evolved granites have difficulty tracing their initial magma compositions as well as their sources [67,68]. In the protolith discrimination diagrams, the low-degree-evolved Shaziling granites mainly plot in the field of metabasaltictometatonalitic sources (hybridization of high-Al olivine tholeiite with metagraywacke), with a small number plotting in the field of metagraywackes (graywacke-derived), indicating that they possibly have protoliths of metaigneous rocks and a minor contribution of metasedimentary rocks (Figure 11a–c). Combining the previous studies, we consider that protoliths of lowercrustal granuliticmetabasaltic rocks with minor metagraywacke input should be appropriate.

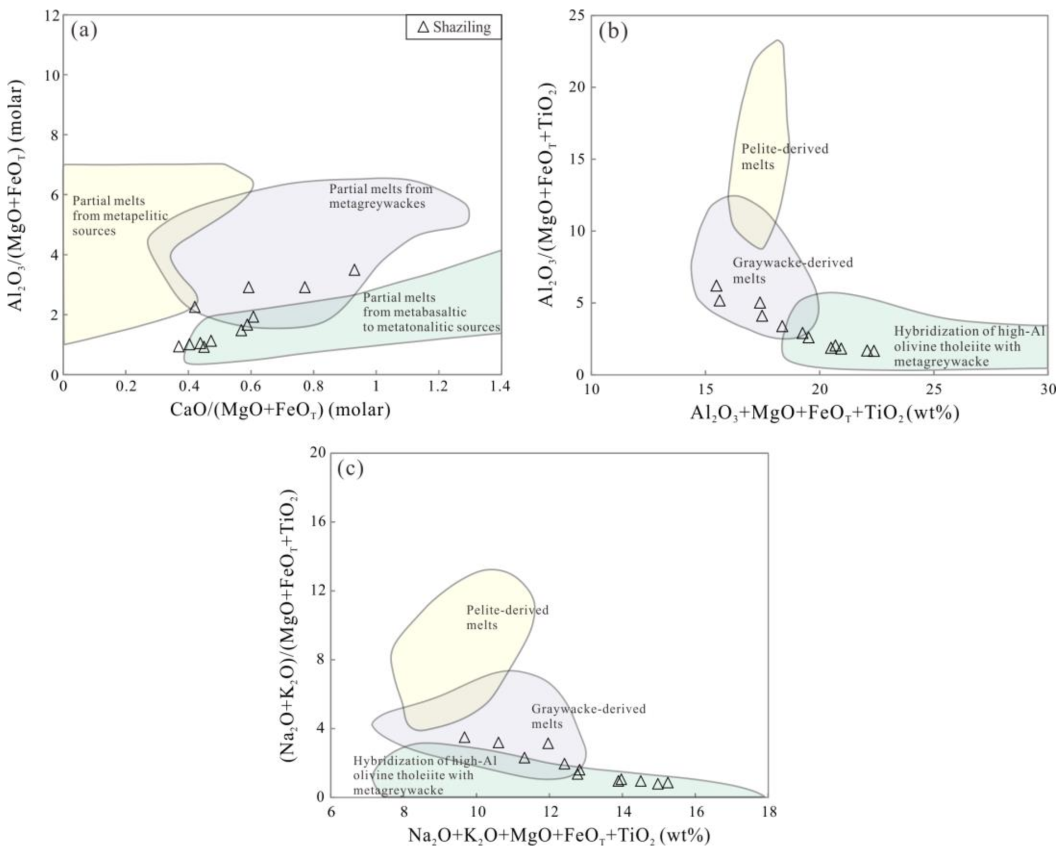

Figure 11. Protolith discrimination diagrams of the studied granitic rocks: (**a**) CaO/(MgO + $Fe_2O_3^T$) vs. Al_2O_3/(MgO+ $Fe_2O_3^T$) (in molar, after Altherr et al. [69]); (**b**) Al_2O_3 + MgO + FeO^T + TiO_2 vs. Al_2O_3/(MgO + FeO^T + TiO_2) (after Patiño Douce, [70]). (**c**) Na_2O + K_2O + MgO + FeO^T + TiO_2 vs. (Na_2O + K_2O)/(MgO + FeO^T + TiO_2) (after Patiño Douce, [70]).

Four units of the Jiuyishan complex massif show narrow whole-rock εNd(t) values and zircon εHf(t) values similar to the lower crust [71]. Combined with no MMEs discovered in the Jinjiling, Pangxiemu and Xishan granites, a magma-mixing process can be avoided in these three units. The Shaziling granites and granodiorites also have similar εNd(t) values and zircon εHf(t) values to their host rocks. However, abundant MMEs were developed inside the host rocks with clear shapes and boundaries. Although their whole-rock εNd(t) values were not analyzed, their major and trace elements exhibit intermediate rock characters, and the zircon εHf(t) values from the MME samples have a wide range of variations between −14.2 and 4.8. The highest zircon εHf(t) value of 4.8 is close to the calculated εHf(t) value of 6.7 (εHf(t) = 1.55 × εNd(t) + 1.21 if not decoupled [72]) from the contemporary dolerite, which is considered to have originated from the enriched mantle [37]. This evidence strongly supports that a mantle magma injection has occurred in the Shaziling granitic magma. However, magma mixing cannot fully explain the process because both the whole-rock εNd(t) values and zircon εHf(t) values of the Shaziling host granites are still consistent with the Xishan, Jinjiling and Pangxiemu granites. Due to the fact that the MMEs are only discovered in a small part of the Shaziling pluton, rather than commonly appearing in all the samples distributed in every part of the pluton, we preferred a mantle magma recharge process, which triggered a local mixing.

Compared to the Shaziling MMEs, the Shaizling granodiorite host rock samples have relatively consistent zircon εHf(t) values between −7.5 and −4.7. The lack of evidence in the Shaziling host rocks, such as wall rock xenoliths, inherited zircons and variable whole-rock εNd(t) and zircon εHf(t) values, could hardly prove a contamination or assimilation of more mature crustal materials. The MMEs are proven to be formed by mantle magma recharge, but the lowest zircon εHf(t) value of −14.2 indicates zircons from mature crustal materials. This evidence proves that the crustal contamination may have occurred in the mantle-derived magmas prior to the recharging process.

Four units of the Jiuyishan complex massif not only have consistent zircon U-Pb ages but also similar whole-rock εNd(t) and zircon εHf(t) values. However, their major and trace elements show a continuous evolutionary trend. The Shaziling, Xishan, Jinjiling and Pangxiemu granites have gradually increased SiO_2 contents, but decreased CaO, MgO, $Fe_2O_3{}^T$, P_2O_5 and TiO_2 contents (Figure 12a–i), which indicates that they experienced the fractionation of amphibole, biotite, ilmenite, titanite, feldspar, titanite and apatite. Moreover, increases in Rb, Nb, Ta, Y and U contents and decreases in Ba, Sr and Eu contents are observed (Figure 8), indicating the fractionation of plagioclase and alkali feldspar and the accumulation of crystallization of columbite, pyrochlore, thorite, monazite and xenotime, which can partly be seen in the Pangxiemu granites as interstitial minerals or mineral inclusions [34,73,74]. The intensive fractionation of feldspars is also proven by a discovery that A-type granites have especially highly stable Ca isotope compositions, likely the result of the rapid or extensive crystallization of plagioclase [75]. Whole-rock Zr/Hf, Rb/Sr and K/Rb ratios commonly serve as efficient criteria to determine the influence of fractional crystallization [6,76,77]. The Shaziling, Xishan, Jinjiling and Pangxiemu granites have gradually increased Rb/Sr ratios, but decreased Zr/Hf and K/Rb ratios (Figure 13a,b). For petrography observations, Shaziling has lithologies of granodiorite and biotite granite, Xishan has biotite granite, Jinjiling has biotite granite and Pangxiemu has zinnwaldite granite. All the evidence listed above indicates a fractional crystallization trend from the Shaziling, Xishan, Jinjiling to Pangximu granites. The Pangximu granites with flat V-shaped REE distribution patterns, which are also extremely depleted in Eu, Ba, Sr, P, Ti, Ca, Mg and Fe contents but enriched in Rb, U, Y, Ta and Nb contents, are typical features of highly evolved granites [10].

To better constrain the magma fractionation of the Jiuyishan complex massif, Rayleigh fractionation crystallization modeling was carried out and Ba, Sr and Rb were selected for modeling; the partition coefficients are presented in Supplementary Table S7. The less-evolved Shaziling granodiorite sample (Rb = 204 ppm; Ba = 1385 ppm; Sr = 158 ppm) was regarded as the initial magma, which has a mineral assemblage of 25% quartz +35% K-feldspar +25% plagioclase +10% biotite +5% amphibole. The modeling result shows that the Shaziling granites also experienced approximately 0%–30% fractionation; approximately 10%−40% fractionation is needed to form the Xishan granites, approximately 20%−70% fractionation is needed to form the Jinjiling granites, and approximately 70%−90% fractionation is needed to form the Pangxiemu granites (Figure 14a,b). However, this result is unrealistic in nature. In a crystal mush system, the less-evolved granites are inferred to represent a residual crystal mush comprising the cumulate crystals and a proportion of highly fractionated interstitial melts, whereas the high-silica granites represent the extracted, highly fractionated interstitial liquid from a crystal mush [15]. We therefore suggest that the composition of the extracted liquid is the same as that of the most evolved Pangxiemu granite sample, and the composition of the residual crystal mush approximates the average composition of the Shaziling, Xishan and Jinjiling granites. According to this model, approximately 60%−80% fractionation is needed to form the Pangxiemu granites (Figure 14a,b).

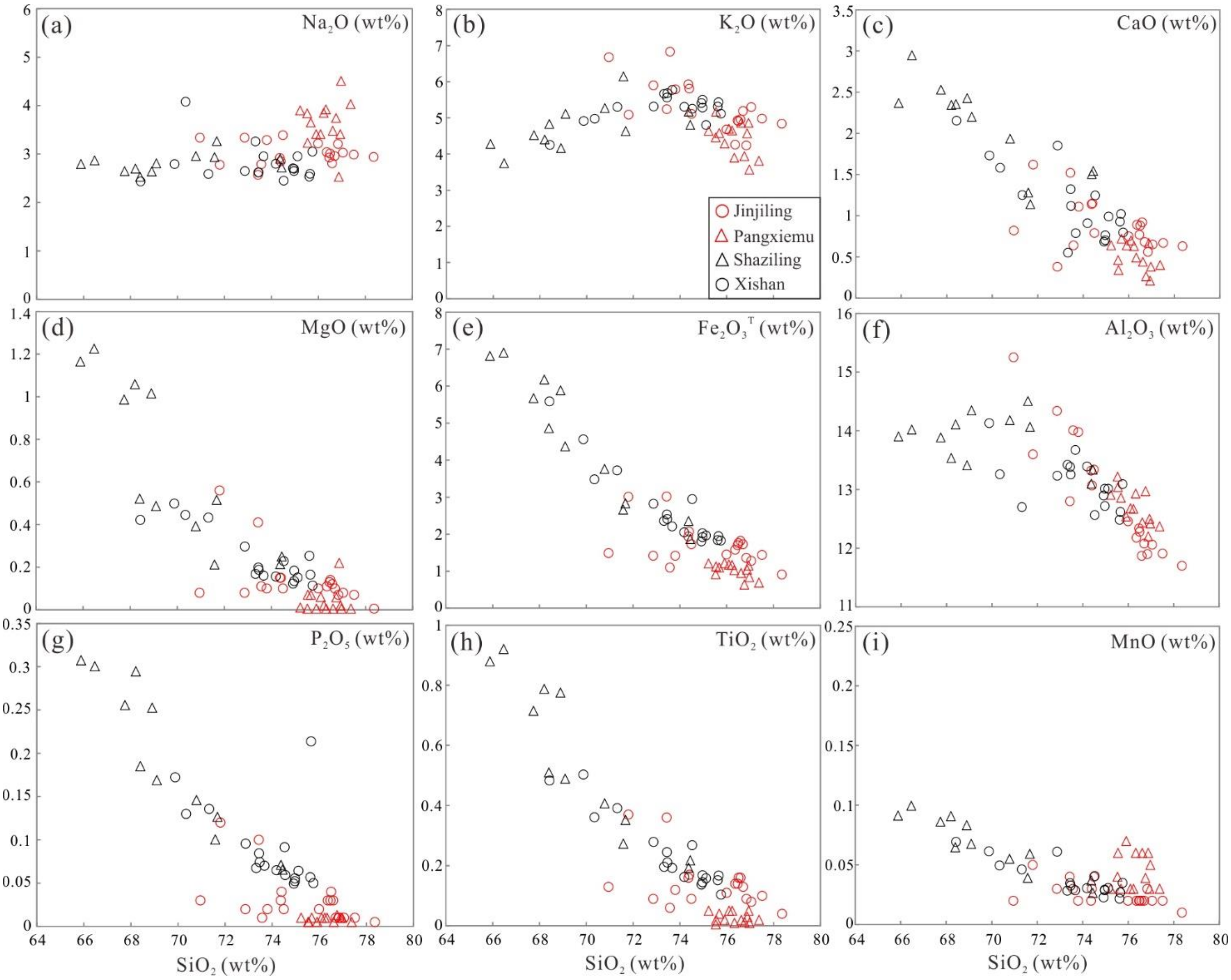

Figure 12. Binray diagrams of the Jiuyishan complex massif: (**a**) SiO_2 vs. Na_2O; (**b**) SiO_2 vs. K_2O; (**c**) SiO_2 vs. CaO; (**d**) SiO_2 vs. MgO; (**e**) SiO_2 vs. $Fe_2O_3{}^T$; (**f**) SiO_2 vs. Al_2O_3; (**g**) SiO_2 vs. P_2O_5; (**h**) SiO_2 vs. TiO_2; (**i**) SiO_2 vs. MnO.

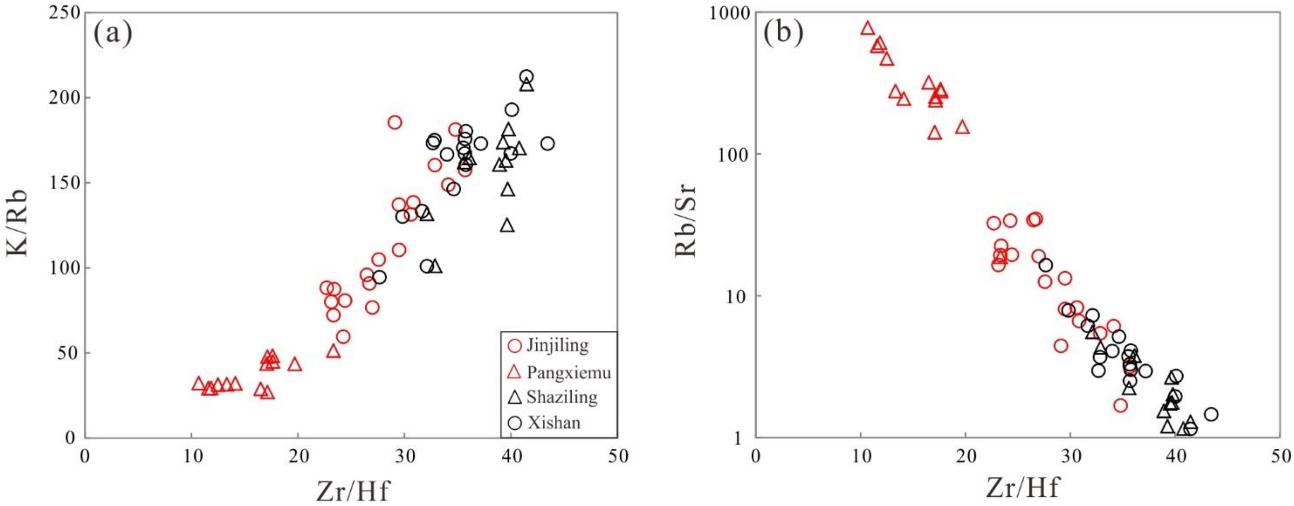

Figure 13. Whole-rock (**a**) Zr/Hf vs. K/Rb and (**b**) Zr/Hf vs. Rb/Sr diagrams of the Jiuyishan complex massif.

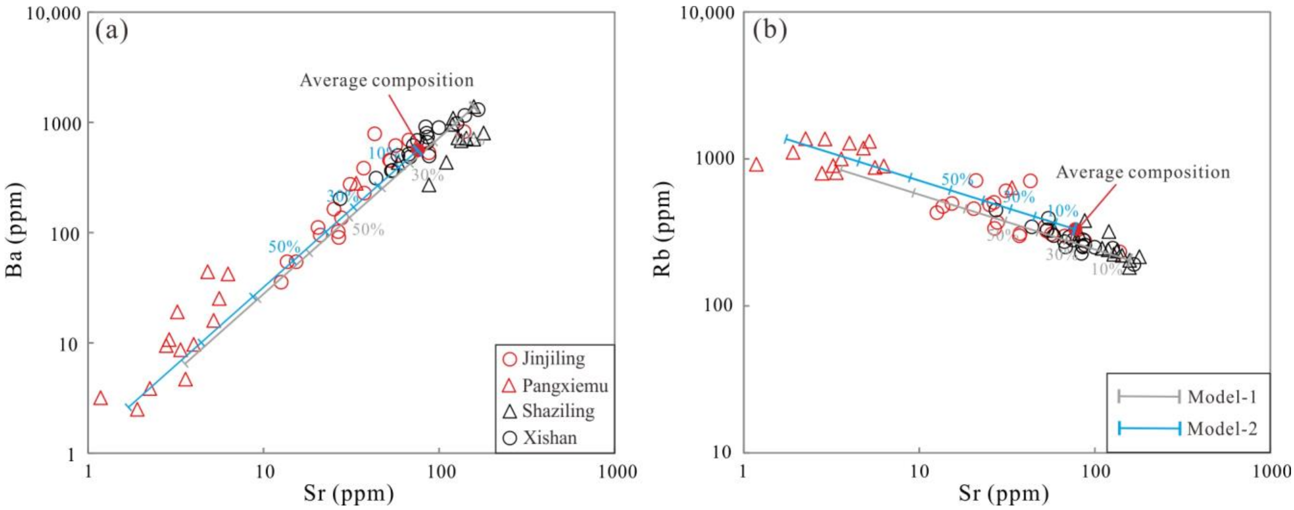

Figure 14. Binray diagrams and Rayleigh fractionation crystallization modelling of (**a**) Sr vs. Ba and (**b**) Sr vs. Rb for the Jiuyishan complex massif. The gray and light-blue arrows represent the two types of predicted chemical evolution.

Therefore, we consider that four units of the Jiuyishan complex massif share the same source region and protoliths in the lower crust. They experienced remarkable fractional crystallization and local mantle magma recharge during their formation.

5.3. Petrogenesis of the Xianghualing Intrusive Stocks

Although the Laiziling and Jianfengling intrusive stocks have a 5 Myr age gap, they have similar isotopic compositions of whole-rock εNd(t) values (−6.5 to −5.7) and zircon εHf(t) values (−7.6 to −2.7), which are also similar to four units from the Jiuyishan complex, indicating their close isotopic compositions of the source region, and they may have analogous source regions in the lower crust. However, since the Laiziling and Jianfengling stocks are highly fractionated, even though the biotite granites at the bottom show highly evolved features [19,38], it is quite difficult to trace their protoliths via major and trace elements. However, compared to the Pangximu granites, Laiziling and Jianfengling granites have similar trace element features but much higher A/CNK values; this may be indicative of a more metasedimentary source, and possibly lower-crustal granulitic metasedimentary rocks.

The Laiziling and Jianfengling intrusive stocks contain different lithologies from the bottom of the rock body to the top with gradual boundaries, indicating a continuous fractional crystallization process [17]. Although topaz granite and greisen at the top of the rock bodies were not collected in this study, zinnwaldite granite in the middle of the rock bodies and biotite granite at the bottom all demonstrate highly evolved characteristics. Flat V-shaped REE distribution patterns, with extremely depleted Eu, Ba, Sr, P, Ti, Ca, Mg and Fe contents but enriched Rb, U, Y, Ta and Nb contents (Figures 8 and 15), are also observed in the Laiziling and Jianfengling biotite and zinnwaldite granites. However, zinnwaldite granites have relatively higher K, Al, Rb, Nb and Ta contents but lower Ti, Fe, Ca, Ba and Sr contents (Figures 8 and 15), and fractionation from biotite to zinnwaldite granites can be confirmed despite their similar major elements and REE distribution patterns.

The Jianfengling and Laiziling granites have remarkable depletions in Mg, Fe, Ca, Ti and P, which may indicate the fractionation of amphibole, biotite, ilmenite, feldspar, titanite and apatite. Moreover, the depletions in Sr, Ba and Eu and the enrichment in Rb represent the fractionation of plagioclase and alkali feldspar. Incompatible elements tend to be crystallized in late-evolved melts, which caused the highly evolved Jianfengling and Laiziling granites to be enriched in Nb, Ta, Th, U, Hf, Y and crystallized columbite, pyrochlore, thorite, monazite and xenotime, which can partly be seen as interstitial minerals or mineral inclusions in the Jianfengling and Laiziling granites [22,40,42,44,45,78].

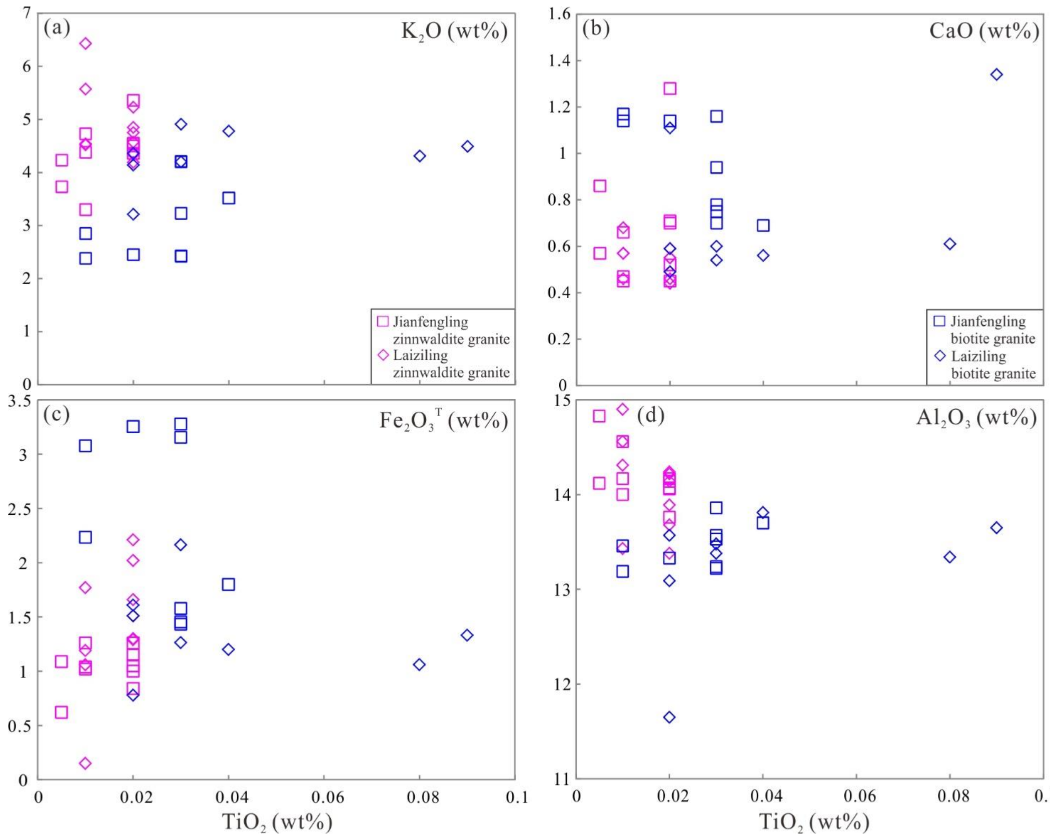

Figure 15. Binray diagrams of the Xianghualing intrusive stocks: (**a**) TiO_2 vs. K_2O; (**b**) TiO_2 vs. CaO; (**c**) TiO_2 vs. $Fe_2O_3{}^T$; (**d**) TiO_2 vs. Al_2O_3.

An assimilation process might have occurred in the Laiziling and Jianfengling highly evolved granites. We consider that these two intrusive stocks might have experienced an assimilation process for the following reasons: (1) Previous studies proved that the highly evolved granites commonly accompany AFC processes [66]. (2) A large dolomite xenolith was found in the interior of the Laiziling stock [79], which was strongly altered by high temperature hydrothermal, indicating it was captured earlier at the magmatic–hydrothermal stage, and it might be assimilated in a small proportion within a local dimension. (3) Abundant inherited zircons were discovered in the Laiziling and Jianfengling granites, which were considered as captured zircons by the assimilation of concealed granites with older ages [42]. (4) The Pb isotope of one Jianfengling granite sample exhibited an upper crustal signature, indicating the incorporation of more mature crustal materials (Figure 9e,f), but a post-magmatic alteration could also have caused the change in Pb isotopes.

In summary, the Laiziling and Jianfengling stocks also have a lower crustal source region. During their formation, a remarkable fractionation crystallization process occurred, accompanied possibly by an assimilation process.

5.4. Different Fractional Crystallization Mechanisms between the Jiuyishan Complex and the Xianghualing Stocks

The mechanism of fractional crystallization remains controversial, especially in felsic magmas. Multiple mechanisms have been proposed by previous studies, such as gravitational settling, flowage differentiation and thermal diffusion or convective fractionation [68,80]. However, such mechanisms are based on mafic magmas, and felsic magmas may not be suitable for these mechanisms [68]. However, some studies also argue that F and other volatiles can remarkably reduce magma viscosity, with clear evidence showing that abundant flow structures were found in field observations of granite systems and that flowage differentiation and gravitational settling can also occur as fractional crystallization mechanisms of felsic magmas [17,18,80]

Recently, a crystal mush system has been proposed to explain the existence of granitic rocks with spatially and temporally related, high-silica rhyolites: large silicic magma chambers are widely perceived as upper crustal mush at a high crystallinity, and these magma chambers are commonly placed into two closely spatio-temporally related crystal-poor and crystal-rich units, respectively [15,58]. The crystal mush system can also be used to interpret the formation of complex massifs. We consider four units of the Jiuyishan complex massif as a crystal mush system for the following reasons: (1) The four units have similar ages and are spatially connected. (2) A fractional crystallization trend was observed from the Shaziling, Xishan, Jinjiling to Pangximu granites, and the Pangxiemu unit is highly evolved. (3) Although the less evolved Shaziling unit is located in the central part of the complex, between the Jinjiling and Xishan units, the northern part extends to the further periphery (Figure 2), indicating that the actual distribution of the unexposed Shaziling unit is the most peripheral. The exposed Shaziling unit may only represent a branch of the magma chamber that inserts into the Jinjiling and Xishan units. (4) The Pangxiemu, Jinjiling, Xishan and Shaziling units are distributed spatially from the top to the bottom and from the central to the margin. A less evolved trend was observed among them, also corresponding to the model of the crystal mush system. (5) The outermost Shaziling unit experienced a mantle magma injection, representing the magma recharge of the magma chamber. Due to the recharging or heating of mafic magmas with high temperatures, the Shaziling granite is medium-to-fine-grained and lacks phenocrysts. Meanwhile, the Xishan and Jinjiling granites are coarse-grained and enriched in feldspar phenocrysts, representing crystal-rich residual mush. The highly evolved Pangxiemu granite is also fine-grained and lacks phenocrysts, representing a crystal-poor extract melt.

The Laiziling and Jianfengling stocks have vertical zonation with different lithologies from the bottom to the top. However, even though the deep drill hole samples at the bottom are still biotite granites with highly evolved features, the low-degree-evolved unit cannot be found. Liu et al. [80] considered that the vertical zonation of granitic rocks can be caused by three mechanisms: (1) flowage differentiation during magma ascent; (2) gravitational settling during magma solidification after emplacement; and (3) gravitational settling in the magma chamber in situ. However, the last mechanism can be precluded because the Laiziling and Jianfengling stocks have an age gap of 5 myrs, which means they cannot share the same magma chamber and separately experience gravitational settling at the same time. If they do not share the same large magma chamber, this means that these adjacent stocks may have isolated small magma chambers. However, they have small, exposed areas and their unfractionated cumulates cannot be found, indicating deep and large concealed parts, and this is in conflict with the small magma chambers. Hence, we consider that the vertical zonation of Laiziling and Jianfengling stocks is more likely caused by flowage differentiation during magma ascent or gravitational settling during magma solidification. Some researchers discovered that many highly evolved granites in the Nanling Range have the phenomenon of vertical zonation, and most of them are small intrusive stocks. They consider that the vertical zonation of these stocks is mainly caused by gravitational settling during magma solidification after emplacement [18], and multiple, later acidic dikes evolved from more fractionated magma can cut the previously emplaced stocks [38,78,81]. Some authors also argue that granitic dikes were formed by long-distance magma emplacement because magma ascends from deep to shallow, usually in the form of dikes [82]. Multiple acidic dikes were found to have developed around the Laiziling stocks, which also verified these theories: they were either formed by evolving from more fractionated magma or long-distance magma emplacement.

Although a series of studies have been proposed to prove the different fractional crystallization mechanisms between the Jiuyishan complex and the Xianghualing stocks, previous studies have considered that the formation of granitic rocks was not only controlled by one mechanism, but a combined action of multiple mechanisms [77]. A simple model can be proposed to demonstrate the formation of the Jiuyishan complex massif and Xianghualing intrusive stocks (Figure 16). Although no vertical zonation has been observed in four units of the Jiuyishan complex massif, the initial magma that formed their magma chamber can also experience flowage differentiation. In comparison, the Laiziling and Jianfengling stocks can also be formed via the re-intruding of the highly evolved extract melt of a preformed crystal mush system in a hidden magma chamber. In summary, fractional crystallization of the Jiuyishan complex massif is mainly controlled by an in situ crystal mush fractionation, while the Xianghualing intrusive stocks are mainly controlled by flowage differentiation during magma ascent or gravitational settling during magma solidification after emplacement. However, more than one mechanism can act on the fractional crystallization processes of granitic rocks.

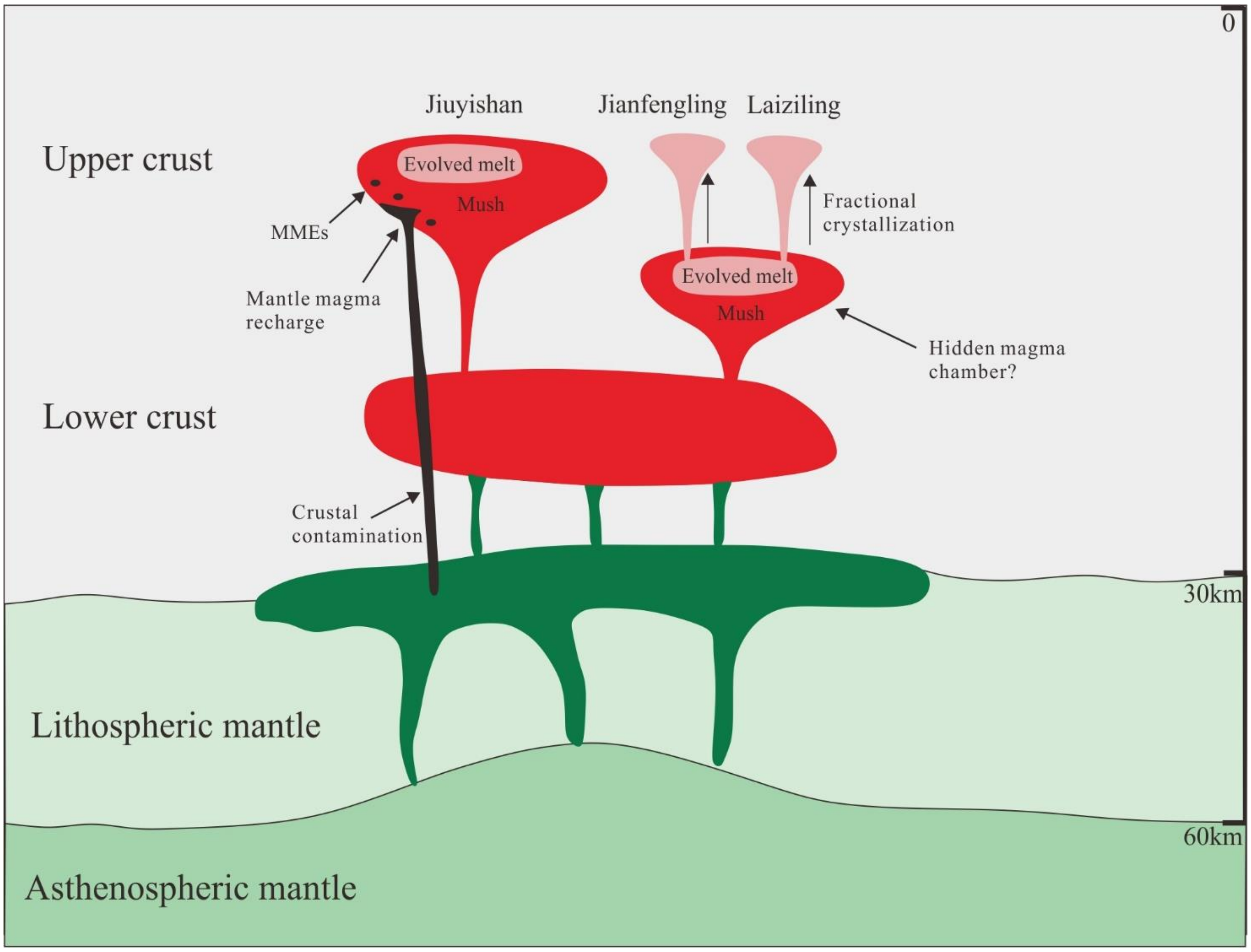

Figure 16. Schematic model showing the petrogenesis of studied magmatic rocks.

6. Conclusions

(1) The Jiuyishan complex massif and Xianghualing intrusive stocks are A_2-type granites with ages between 160 and 150 Ma.

(2) The Jiuyishan complex massif has a source region that is linked to the lower crustal granulitic metabasaltic rocks; they experienced fractional crystallization and mantle magma recharge during their formation.

(3) The Jianfengling and Laiziling intrusive stocks also have similar source regions in the lower crust; they experienced remarkable fractionation crystallization, accompanied with possible assimilation.

(4) The fractional crystallization mechanism of the Jiuyishan complex massif was mainly controlled by in situ crystal mush fractionation, while the Xianghualing intrusive stocks were mainly controlled by flowage differentiation during magma ascent or gravitational settling during magma solidification after emplacement.

Supplementary Materials: The following supporting information can be downloaded at: https://www.mdpi.com/article/10.3390/min13050605/s1. Supplementary Table S1. Zircon LA-ICP-MS U-Pb dating results. Supplementary Table S2. Inherited zircon LA-ICP-MS U-Pb dating results of the Jianfengling and Laiziling granites. Supplementary Table S3. Zircon LA-MC-ICP-MS Hf isotopic compositions. Supplementary Table S4. Whole-rock major (wt%) and trace (ppm) element compositions. Supplementary Table S5. Whole-rock Sr and Nd isotopic compositions. Supplementary Table S6. Whole-rock Pb isotopic compositions of Jianfengling and Laiziling granites. Supplementary Table S7. Used partition coefficients of elements between mineral and melt in Rayleigh fractionation crystallization modeling.

Author Contributions: Conceptualization, W.X.; methodology, W.X.; software, M.S.; validation, M.S.A.; formal analysis, W.X.; investigation, W.X. and C.L.; data curation, C.L.; writing—original draft, W.X.; writing—review and editing, K.S., Q.S., P.F. and M.S.; funding acquisition, W.X., X.D., M.S.A. and F.Z. Project administration, K.T., X.D. and F.Z. All authors have read and agreed to the published version of the manuscript.

Funding: This study was financially supported by Open Research Fund Program of Fundamental Science on Radioactive Geology and Exploration Technology Laboratory (East China University of Technology) (2022RGET04), Researchers Supporting Project number (RSP 2023R455), King Saud University, Riyadh, Saudi Arabia, Provincial Natural Science Foundation of Hunan (2019JJ50831), China Postdoctoral Science Foundation (2017M622597; 2021M690591), National Foreign Expert Project (G2022029012L) and National Nature Science Foundation of China (41002022).

Data Availability Statement: Not applicable.

Acknowledgments: We appreciate Quan Ou, Ye Liu, Shuanglian Li and Rijun Du for the field support. Editor and four anonymous reviewers are much acknowledged for their constructive comments, which greatly helped to improve this manuscript.

Conflicts of Interest: The authors declare no conflict of interest.

References

1. Loiselle, M.C.; Wones, D.R. Characteristics and origin of anorogenic granites. *Geol. Soc. Am. Abstr. Programs* **1979**, *11*, 468.
2. Huang, H.Q.; Li, X.H.; Li, W.X.; Li, Z.X. Formation of high 18O fayalite-bearing A-type granite by high-temperature melting of granulitic metasedimentary rocks, southern China. *Geology* **2011**, *39*, 903–906. [CrossRef]
3. Guo, C.; Zeng, L.; Li, Q.; Fu, J.; Ding, T. Hybrid genesis of Jurassic fayalite-bearing felsic subvolcanic rocks in South China: Inspired by petrography, geochronology, and Sr–Nd–O–Hf isotopes. *Lithos* **2016**, *264*, 175–188. [CrossRef]
4. Abdel-Karim, A.-A.; Azer, M.; Sami, M. Petrogenesis and tectonic implications of the Maladob ring complex in the South Eastern Desert, Egypt: New insights from mineral chemistry and whole-rock geochemistry. *Int. J. Earth Sci.* **2020**, *110*, 53–80. [CrossRef]
5. Peng, H.-W.; Fan, H.-R.; Jiang, P.; Hu, H.-L.; Lan, T.-G. Two-stage rollbacks of the paleo-Pacific plate beneath the Cathaysia block during Cretaceous: Insights from A-type granites and volcanic rocks. *Gondwana Res.* **2021**, *97*, 158–175. [CrossRef]
6. Sami, M.; El Monsef, M.A.; Abart, R.; Toksoy-Köksal, F.; Abdelfadil, K.M. Unraveling the Genesis of Highly Fractionated Rare-Metal Granites in the Nubian Shield via the Rare-Earth Elements Tetrad Effect, Sr–Nd Isotope Systematics, and Mineral Chemistry. *ACS Earth Space Chem.* **2022**, *6*, 2368–2384. [CrossRef]
7. Zhou, Y.; Liang, X.; Wu, S.; Cai, Y.; Liang, X.; Shao, T.; Wang, C.; Fu, J.; Jiang, Y. Isotopic geochemistry, zircon U–Pb ages and Hf isotopes of A-type granites from the Xitian W–Sn deposit, SE China: Constraints on petrogenesis and tectonic significance. *J. Asian Earth Sci.* **2015**, *105*, 122–139. [CrossRef]
8. Zheng, W.; Mao, J.-W.; Zhao, H.-J.; Ouyang, H.-G.; Zhao, C.-S.; Yu, X.-F. Geochemistry, Sr–Nd–Pb–Hf isotopes systematics and geochronological constrains on petrogenesis of the Xishan A-type granite and associated W–Sn mineralization in Guangdong Province, South China. *Ore Geol. Rev.* **2017**, *88*, 739–752. [CrossRef]
9. Yang, L.; Wu, X.; Cao, J.; Hu, B.; Zhang, X.; Gong, Y.; Liu, W. Geochronology, petrology, and genesis of two granitic plutons of the Xianghualing ore field in south Hunan province: Constraints from zircon U–Pb dating, geochemistry, and Lu–Hf isotopic compositions. *Minerals* **2018**, *8*, 213. [CrossRef]

10. Liu, Y.; Lai, J.; Xiao, W.; Jeffrey, D.; Du, R.; Li, S.; Liu, C.; Wen, C.; Yu, X. Petrogenesis and Mineralization of Two-Stage A-Type Granites in Jiuyishan, South China: Constraints from Whole-rock Geochemistry, Mineral Composition and Zircon U-Pb-Hf Isotopes. *Acta Geol. Sin.-Engl. Ed.* **2019**, *93*, 874–900. [CrossRef]
11. Sami, M.; Mahdy, N.M.; Ntaflos, T.; Fathy, D. Composition and origin of Ti–Nb–Ta–Zr bearing minerals in the Abu Diab highly evolved granite from the Central Eastern Desert of Egypt. *J. Afr. Earth Sci.* **2020**, *165*, 103808. [CrossRef]
12. Shu, X.-J.; Wang, X.-L.; Sun, T.; Xu, X.; Dai, M.-N. Trace elements, U–Pb ages and Hf isotopes of zircons from Mesozoic granites in the western Nanling Range, South China: Implications for petrogenesis and W–Sn mineralization. *Lithos* **2011**, *127*, 468–482. [CrossRef]
13. Li, H.; Palinkaš, L.A.; Watanabe, K.; Xi, X.-S. Petrogenesis of Jurassic A-type granites associated with Cu-Mo and W-Sn deposits in the central Nanling region, South China: Relation to mantle upwelling and intra-continental extension. *Ore. Geol. Rev.* **2018**, *92*, 449–462. [CrossRef]
14. Wang, L.-X.; Ma, C.-Q.; Zhang, C.; Zhang, J.-Y.; Marks, M.A. Genesis of leucogranite by prolonged fractional crystallization: A case study of the Mufushan complex, South China. *Lithos* **2014**, *206*, 147–163. [CrossRef]
15. Chen, S.-C.; Yu, J.-J.; Bi, M.-F. Extraction of fractionated interstitial melt from a crystal mush system generating the Late Jurassic high-silica granites from the Qitianling composite pluton, South China: Implications for greisen-type tin mineralization. *Lithos* **2021**, *382*, 105952. [CrossRef]
16. Liao, Y.; Zhao, B.; Zhang, D.; Danyushevsky, L.V.; Li, T.; Wu, M.; Liu, F. Evidence for temporal relationship between the late Mesozoic multistage Qianlishan granite complex and the Shizhuyuan W-Sn-Mo-Bi deposit, SE China. *Sci. Rep.* **2021**, *11*, 5828. [CrossRef]
17. Xiong, X.-L.; Rao, B.; Chen, F.-R.; Zhu, J.-C.; Zhao, Z.-H. Crystallization and melting experiments of a fluorine-rich leucogranite from the Xianghualing Pluton, South China, at 150 MPa and H2O-saturated conditions. *J. Asian Earth Sci.* **2002**, *21*, 175–188. [CrossRef]
18. Zhu, J.; Rao, B.; Xiong, X.; Li, F.; Zhang, P. Comparison and genetic interpretation of Li-F rich, rare-metal bearing granitic rocks. *Geochimica* **2002**, *31*, 141–152, (In Chinese with English Abstract).
19. Zhu, J.; Wang, R.; Lu, J.; Zhang, H.; Zhang, W.; Xie, L.; Zhang, R. Fractionation, evolution, petrogenesis and mineralization of Laiziling granite pluton, southern Hunan Province. *Geol. J. China Univ.* **2011**, *17*, 381, (In Chinese with English Abstract).
20. Wen, C.; Shao, Y.; Huang, G.; Luo, X.; Li, S. Geochemical features of Jianfengling rare metal granite in Hunan Province. *Miner. Depos.* **2017**, *36*, 879–892, (In Chinese with English Abstract).
21. Huang, W.; Wu, J.; Liang, H.; Zhang, J.; Ren, L.; Chen, X. Ages and genesis of W-Sn and Ta-Nb-Sn-W mineralization associated with the Limu granite complex, Guangxi, China. *Lithos* **2020**, *352–353*, 105321. [CrossRef]
22. Che, X.-D.; Wang, R.-C.; Wu, F.-Y.; Zhu, Z.-Y.; Zhang, W.-L.; Hu, H.; Xie, L.; Lu, J.-J.; Zhang, D. Episodic Nb–Ta mineralisation in South China: Constraints from in situ LA–ICP–MS columbite–tantalite U–Pb dating. *Ore. Geol. Rev.* **2018**, *105*, 71–85. [CrossRef]
23. Zhang, S.-B.; Zheng, Y.-F. Formation and evolution of Precambrian continental lithosphere in South China. *Gondwana Res.* **2013**, *23*, 1241–1260. [CrossRef]
24. Zhao, G. Jiangnan Orogen in South China: Developing from divergent double subduction. *Gondwana Res.* **2015**, *27*, 1173–1180. [CrossRef]
25. Xia, Y.; Xu, X.; Niu, Y.; Liu, L. Neoproterozoic amalgamation between Yangtze and Cathaysia blocks: The magmatism in various tectonic settings and continent-arc-continent collision. *Precambrian Res.* **2018**, *309*, 56–87. [CrossRef]
26. Hacker, B.R.; Ratschbacher, L.; Liou, J. Subduction, collision and exhumation in the ultrahigh-pressure Qinling-Dabie orogen. *Geol. Soc. Lond. Spec. Publ.* **2004**, *226*, 157–175. [CrossRef]
27. Zheng, Y. A perspective view on ultrahigh-pressure metamorphism and continental collision in the Dabie-Sulu orogenic belt. *Chin. Sci. Bull.* **2008**, *53*, 3081–3104. [CrossRef]
28. Chang, E.Z. Geology and tectonics of the Songpan-Ganzi fold belt, southwestern China. *Int. Geol. Rev.* **2000**, *42*, 813–831. [CrossRef]
29. Enkelmann, E.; Weislogel, A.; Ratschbacher, L.; Eide, E.; Renno, A.; Wooden, J. How was the Triassic Songpan-Ganzi basin filled? A provenance study. *Tectonics* **2007**, *26*. [CrossRef]
30. Mao, J.W.; Xie, G.Q.; Guo, C.L.; Chen, Y.C. Large-scale tungstentin mineralization in the Nanling region, South China: Metallogenic ages and corresponding geodynamic processes. *Acta Petrol. Sin.* **2007**, *23*, 2329–2338, (In Chinese with English Abstract).
31. Ou, Q.; Lai, J.-Q.; Carvalho, B.B.; Zi, F.; Jiang, Z.-Q.; Wang, K.; Liu, Y.-Z. Early Silurian granitic rocks and associated enclaves as evidence of rapid cooling in a cognate magma system: The case of the Xuehuading–Panshanchong pluton, South China Block. *Geol. Mag.* **2020**, *158*, 1173–1193. [CrossRef]
32. Fu, J.; Ma, C.; Xie, C.; Zhang, Y.; Peng, S. SHRIMP U-Pb zircon dating of the Jiuyishan composite granite in Hunan and its geological significance. *Geotecton. Metallogen.* **2004**, *28*, 370–378, (In Chinese with English Abstract).
33. Kong, H.; Wu, J.-H.; Li, H.; Chen, S.-F.; Liu, B.; Wang, G. Early Paleozoic tectonic evolution of the South China Block: Constraints from geochemistry and geochronology of granitoids in Hunan Province. *Lithos* **2021**, *380*, 105891. [CrossRef]
34. Su, H. The Petrogenesis Studies of the Mesozoic Xiangyuan Tungsten-Tin Deposit and Related Granites in Hunan Province. Master's Thesis, China University of Geosciences (Beijing), Beijing, China, 2017; pp. 1–84, (In Chinese with English Abstract).
35. Li, J.; Sheng, H.; You, S. Zircon U–Pb ages, geochemistry, Sr–Nd–Hf isotopic compositions, and geological implications of the Shaziling pluton in the Nanling Orogenic Belt, southern China. *Geol. J.* **2020**, *55*, 6749–6764. [CrossRef]

36. Jiang, Y.-H.; Jiang, S.-Y.; Dai, B.-Z.; Liao, S.-Y.; Zhao, K.-D.; Ling, H.-F. Middle to late Jurassic felsic and mafic magmatism in southern Hunan province, southeast China: Implications for a continental arc to rifting. *Lithos* **2009**, *107*, 185–204. [CrossRef]
37. Du, R.; Lai, J.; Ou, Q.; Xiao, W.; Liu, Y.; Liu, C.; Li, S. Petrogenesis of the Jinjiling Diabasic Dikes in Southern Hunan and Its Dynamic Significance. *Acta Geol. Sin.* **2019**, *93*, 1998–2019, (In Chinese with English Abstract).
38. Lai, S. Research on mineralization of the Xianghualing tin polymetallic deposit, Hunan Province, China. Ph.D. Thesis, China University of Geosciences (Beijing), Beijing, China, 2014; pp. 1–151, (In Chinese with English Abstract).
39. Xiao, C.; Shen, Y.; Wei, C. Petrogenesis of low Sr and high Yb A-type granitoids in the Xianghualing Sn polymetallic deposit, South China: Constrains from geochronology and Sr–Nd–Pb–Hf isotopes. *Minerals* **2019**, *9*, 182. [CrossRef]
40. Wu, Q.; Feng, C.-Y.; Mao, J.-W.; Santosh, M.; Dick, J.M.; Yu, M.; Li, B. Robust monazite U-Pb and molybdenite Re-Os ages reveal the magmatic and metallogenic history of a highly evolved granitic system in the Xianghualing deposit, South China. *Ore Geol. Rev.* **2022**, *140*, 104602. [CrossRef]
41. Xuan, Y.; Yuan, S.; Yuan, Y.; Mi, J. Zircon U-Pb age, geochemistry and petrogenesis of Jianfengling pluton in southern Hunan Province. *Miner. Depos.* **2014**, *33*, 1379–1390, (In Chinese with English Abstract).
42. Li, H.; Wu, J.-H.; Evans, N.J.; Jiang, W.-C.; Zhou, Z.-K. Zircon geochronology and geochemistry of the Xianghualing A-type granitic rocks: Insights into multi-stage Sn-polymetallic mineralization in South China. *Lithos* **2018**, *312–313*, 1–20. [CrossRef]
43. Wang, Z.; Xie, L.; Wang, R.; Zhu, J.C.; Che, X.; Zhao, X. The petrogenesis and mineralization of the Laiziling greisen, Xianghualing District, Hunan Province, South China. *Geol. J. China Univ.* **2018**, *24*, 467, (In Chinese with English Abstract).
44. Xie, L.; Wang, Z.; Wang, R.; Zhu, J.; Che, X.; Gao, J.; Zhao, X. Mineralogical constraints on the genesis of W–Nb–Ta mineralization in the Laiziling granite (Xianghualing district, south China). *Ore Geol. Rev.* **2018**, *95*, 695–712. [CrossRef]
45. Diao, X.; Wu, M.; Zhang, D.; Liu, J. Textural Features and Chemical Evolution of Ta-Nb-W-Sn Oxides in the Jianfengling Deposit, South China. *Ore Geol. Rev.* **2022**, *142*, 104690. [CrossRef]
46. Qiu, R.; Deng, J.; Cai, Z.; Zhou, S.; Chang, H.; Du, S. Material sources of granite and ore in Xianghualing mult-metal orefield, Hunan Province. *Miner. Depos.* **2002**, *21*, 1017–1020, (In Chinese with English Abstract).
47. Liu, Y.; Gao, S.; Hu, Z.; Gao, C.; Zong, K.; Wang, D. Continental and Oceanic Crust Recycling-induced Melt-Peridotite Interactions in the Trans-North China Orogen: U-Pb Dating, Hf Isotopes and Trace Elements in Zircons from Mantle Xenoliths. *J. Pet.* **2010**, *51*, 537–571. [CrossRef]
48. Hu, Z.; Liu, Y.; Chen, L.; Zhou, L.; Li, M.; Zong, K.; Zhu, L.; Gao, S. Contrasting matrix induced elemental fractionation in NIST SRM and rock glasses during laser ablation ICP-MS analysis at high spatial resolution. *J. Anal. At. Spectrom.* **2011**, *26*, 425–430. [CrossRef]
49. Liu, Y.; Hu, Z.; Zong, K.; Gao, C.; Gao, S.; Xu, J.; Chen, H. Reappraisement and refinement of zircon U-Pb isotope and trace element analyses by LA-ICP-MS. *Chin. Sci. Bull.* **2010**, *55*, 1535–1546. [CrossRef]
50. Hoskin, P.W.O.; Kinny, P.D.; Wyborn, D.; Chappell, B.W. Identifying Accessory Mineral Saturation during Differentiation in Granitoid Magmas: An Integrated Approach. *J. Pet.* **2000**, *41*, 1365–1396. [CrossRef]
51. Belousova, E.; Griffin, W.; Suzanne, Y.O.R.; Fisher, N. Igneous zircon: Trace element composition as an indicator of source rock type. *Contrib. Mineral. Petrol.* **2002**, *143*, 602–622. [CrossRef]
52. Middlemost, E.A.K. Naming materials in the magma/igneous rock system. *Earth-Sci. Rev.* **1994**, *37*, 215–224. [CrossRef]
53. Maniar, P.D.; Piccoli, P.M. Tectonic discrimination of granitoids. *Geol. Soc. Am. Bull.* **1989**, *101*, 635–643. [CrossRef]
54. Frost, B.R.; Barnes, C.G.; Collins, W.J.; Arculus, R.J.; Ellis, D.J.; Frost, C.D. A geochemical classification for granitic rocks. *J. Pet.* **2001**, *42*, 2033–2048. [CrossRef]
55. Sun, S.-S.; McDonough, W.F. Chemical and isotopic systematics of oceanic basalts: Implications for mantle composition and processes. *Geol. Soc. Lond. Spec. Publ.* **1989**, *42*, 313–345. [CrossRef]
56. Zhao, Z.-F.; Gao, P.; Zheng, Y.-F. The source of Mesozoic granitoids in South China: Integrated geochemical constraints from the Taoshan batholith in the Nanling Range. *Chem. Geol.* **2015**, *395*, 11–26. [CrossRef]
57. Zhu, R.-Z.; Lai, S.-C.; Qin, J.-F.; Zhao, S.-W.; Santosh, M. Strongly peraluminous fractionated S-type granites in the Baoshan Block, SW China: Implications for two-stage melting of fertile continental materials following the closure of Bangong-Nujiang Tethys. *Lithos* **2018**, *316–317*, 178–198. [CrossRef]
58. Chen, X.-D.; Li, B.; Yu, M.; Zhang, W.-D.; Zhu, L. Generation of crystal-rich rhyodacites by fluid-induced crystal-mush rejuvenation: Perspective from the Late Triassic Nageng (sub-) volcanic complex of the East Kunlun Orogen, NW China. *Chem. Geol.* **2022**, *599*, 120833. [CrossRef]
59. Sami, M.; Ntaflos, T.; Farahat, E.S.; Mohamed, H.A.; Hauzenberger, C.; Ahmed, A.F. Petrogenesis and geodynamic implications of Ediacaran highly fractionated A-type granitoids in the north Arabian-Nubian Shield (Egypt): Constraints from whole-rock geochemistry and Sr-Nd isotopes. *Lithos* **2018**, *304–307*, 329–346. [CrossRef]
60. Wu, F.Y.; Sun, D.Y.; Li, H.M.; Jahn, B.M.; Wilde, S. A-type granites in northeastern China: Age and geochemical constraints on their petrogenesis. *Chem. Geol.* **2002**, *187*, 143–173. [CrossRef]
61. Sami, M.; Ntaflos, T.; Farahat, E.S.; Mohamed, H.A.; Ahmed, A.F.; Hauzenberger, C. Mineralogical, geochemical and Sr-Nd isotopes characteristics of fluorite-bearing granites in the Northern Arabian-Nubian Shield, Egypt: Constraints on petrogenesis and evolution of their associated rare metal mineralization. *Ore Geol. Rev.* **2017**, *88*, 1–22. [CrossRef]
62. Whalen, J.B.; Currie, K.L.; Chappell, B.W. A-type granites: Geochemical characteristics, discrimination and petrogenesis. *Contrib. Mineral. Petrol.* **1987**, *95*, 407–419. [CrossRef]

63. Eby, G.N. Chemical subdivision of the A-type granitoids:Petrogenetic and tectonic implications. *Geology* **1992**, *20*, 641–644. [CrossRef]
64. Depaolo, D.J. Neodymium Isotopes in the Colorado Front Range and Crust-mantle Evolution in Proterozoic. *Nature* **1981**, *291*, 193–196. [CrossRef]
65. Depaolo, D.J.; Perry, F.V.; Baldridge, W.S. Crustal versus mantle sources of granitic magmas: A two-parameter model based on Nd isotopic studies. *Earth Environ. Sci. Trans. R. Soc. Edinb.* **1992**, *83*, 439–446.
66. Zhao, P.; Alexandrov, I.; Jahn, B.-m.; Liao, J.-P.; Ivin, V. Late Eocene granites in the Central Sakhalin Island (Russian Far East) and its implication for evolution of the Sakhalin-Hokkaido orogenic belt. *Lithos* **2019**, *324*, 684–698. [CrossRef]
67. Chappell, B.W.; White, A.J.R.; Brown, P.E.; Chappell, B.W. I- and S-type granites in the Lachlan Fold Belt. *Earth Environ. Sci. Trans. R. Soc. Edinb.* **1992**, *83*, 1–26.
68. Wu, F.; Liu, X.; Ji, W.; Wang, J.; Yang, L. Highly fractionated granites: Recognition and research. *Sci. China Earth Sci.* **2017**, *60*, 1201–1219, (In Chinese with English Abstract). [CrossRef]
69. Altherr, R.; Holl, A.; Hegner, E.; Langer, C.; Kreuzer, H. High-potassium, calc-alkaline I-type plutonism in the European Variscides: Northern Vosges (France) and northern Schwarzwald (Germany). *Lithos* **2000**, *50*, 51–73. [CrossRef]
70. Patiño Douce, A.E. What do experiments tell us about the relative contributions of crust and mantle to the origin of granitic magmas? *Geol. Soc. Lond. Spec. Publ.* **1999**, *168*, 55–75. [CrossRef]
71. Ping, X.; Zheng, J.; Xiong, Q.; Griffin, W.L.; Yu, C.; Su, Y. Downward rejuvenation of the continental lower crust beneath thesoutheastern North China Craton. *Tectonophysics* **2019**, *750*, 213–288. [CrossRef]
72. Vervoort, J.D.; Plank, T.; Prytulak, J. The Hf–Nd isotopic composition of marine sediments. *Geochim. et Cosmochim. Acta* **2011**, *75*, 5903–5926. [CrossRef]
73. Liu, C.; Lai, J.; Xiao, W.; Zhang, L.; Belousova, E.A.; Rushmer, T.; Xie, F. Formation of Li-Rb-Cs greisen-type deposit in Zhengchong, Jiuyishan district, South China: Constraints from whole-rock and mineral geochemistry. *Geochemistry* **2021**, *81*, 125796. [CrossRef]
74. Liu, X.-H.; Li, B.; Xu, J.-W.; He, B.; Liao, J.; Peng, H.-W.; Wang, Y.-H.; Lai, J.-Q. Monazite geochronology and geochemistry constraints on the formation of the giant Zhengchong Li-Rb-Cs deposit in South China. *Ore Geol. Rev.* **2022**, 105147. [CrossRef]
75. Antonelli, M.A.; Yakymchuk, C.; Schauble, E.A.; Foden, J.; Janousek, V.; Moyen, J.-F.; Hoffman, J.; Moynier, F.; Bachmann, O. Granite petrogenesis and the δ44Ca of continental crust. *Earth Planet. Sci. Lett.* **2023**, *608*, 118080. [CrossRef]
76. Sami, M.; Azer, M.; Abdel-Karim, A.-A. Post-collisional Ferani volcanics from north Arabian-Nubian Shield (south Sinai, Egypt): Petrogenesis and implication for Ediacaran (607–593 Ma) geodynamic evolution. *J. Geol.* **2023**, *in press*. [CrossRef]
77. Sami, M.; Adam, M.M.; Lv, X.; Lasheen, E.S.R.; Ene, A.; Zakaly, H.M.; Alarifi, S.S.; Mahdy, N.M.; Abdel Rahman, A.R.A.; Saeed, A. Petrogenesis and Tectonic Implications of the Cryogenian I-Type Granodiorites from Gabgaba Terrane (NE Sudan). *Minerals* **2023**, *13*, 331. [CrossRef]
78. Huang, F.-F.; Wang, R.-C.; Xie, L.; Zhu, J.-C.; Erdmann, S.; Che, X.-D.; Zhang, R.-Q. Differentiated rare-element mineralization in an ongonite–topazite composite dike at the Xianghualing tin district, Southern China: An electron-microprobe study on the evolution from niobium–tantalum-oxides to cassiterite. *Ore Geol. Rev.* **2015**, *65*, 761–778. [CrossRef]
79. Zhao, Y.; Feng, C.; Li, D.; Liu, J.; Wang, H.; Zhang, S. Li, Be-bearing ribbon rocks and related metasomatites in Xianghualing tin-polymetallic deposit, Hunan Province. *Miner. Depos.* **2019**, *36*, 1245–1262, (In Chinese with English Abstract).
80. Liu, Z.C.; Wu, F.Y.; Liu, X.C.; Wang, J.G. The mechanisms of fractional crystallization for the Himalayan leucogranites. *Acta Petrol. Sin.* **2020**, *6*, 3551–3571.
81. Li, S.-L.; Lai, J.-Q.; Xiao, W.-Z.; Belousova, E.A.; Rushmer, T.; Zhang, L.-J.; Ou, Q.; Liu, C.-Y. Crustal growth event in the Cathaysia Block at 2.5 Ga: Evidence from chronology and geochemistry of captured zircons in Jurassic acidic dykes. *Geol. Mag.* **2021**, *158*, 567–582. [CrossRef]
82. Yamato, P.; Tartese, R.; Duretz, T.; May, D.A. Numerical modelling of magma transport in dykes. *Tectonophysics* **2012**, *526*, 97–109. [CrossRef]